

Reviewer #2 (Anonymous):

We thank this anonymous referee for the set of constructive suggestions. We have revised the text of the manuscript to address most of the referee's suggestions, and feel that this has significantly strengthened the manuscript.

Detailed response to Reviewer #2 Comments (reviewer comments in *italics*, manuscript text underlined)

This manuscript requires some revisions before submitting again. 1) It is quite confusing whether the initial simulation was 2x GFEDv3 or 1x GFEDv3. Are the unadjusted BC emissions 1x or 2x GFEDv3, and the adjusted BC emissions about 2x or 4x GFEDv3? Please clarify.

We acknowledge this confusion. On page 28077 we state “our initial simulations were forced with 2x GFEDv3 BC and OC emissions and 1x GFEDv3 SO₂ emissions,” but recognize that in Table 1 this designation is a bit murky. To remedy this problem, we have added text to Table 1:

Original sum of BC and OC emissions⁵ (Tg yr⁻¹)

⁵ The original BC and OC emissions were 2x GFEDv3 (van der Werf et al., 2010)

2) p. 2807, line 14: The emission factors of Andreae and Merlet (2001) have been updated by several publications, such as Akagi et al., ACP 11, 4039-4072, 2011. What are the differences in BC emission factors of the two publications? Do the differences affect the results of CAM5 simulations? I suggest using Akagi's compiled emission factors to redo CAM5 simulations.

For this study, we used the Global Fire Emissions Database, version 3 (GFEDv3) as our emissions dataset for model simulation initialization. The details of the construction of this dataset are aptly described in van der Werf et al., 2010 and more information can be found on the web at:

<http://www.globalfiredata.org/index.html>. Additionally, we describe in brief the construction of this dataset on page 28076.

We obtained detailed information from G. R. van der Werf on the specific construction of the GFED, version 3 dataset as it concerns the emission factors. GFEDv3 used emission factors from Andreae and Merlet (2001) which are updated by A. Andreae periodically in an excel spreadsheet: available upon request. Specifically, GFEDv3 used updates from 2009 because the dataset was constructed in 2010. The emission factors for BC and OC used in GFEDv3 are listed in the table below (Table 1; also Table 5 in van der Werf et al., 2010):

Table 1. Selected emission factors used in the global fire emissions database, v. 3 by van der Werf et al., 2010 (g/kg)

Species	Deforestation	Savanna	Woodland	Extratrop Forest	Agricul. Waste burning	Peat forest
OC	4.30	3.21	3.76	9.14	3.71	4.30
BC	0.57	0.46	0.52	0.56	0.48	0.57

These numbers are very similar in tropical forest, savanna and extratropical forest ecosystems to those from Akagi et al., 2011 (Table 2; interpreted from Table 1 in Akagi et al., 2011):

Table 2. Selected emission factors presented in Akagi et al., 2011 (g/kg)

Species	Tropical Forest	Savanna	Woodland	Extratrop Forest	Agricultural (crop residue + pasture mainten.)	Peat forest
OC	4.71	2.62	-	8.6 – 9.7	2.30 – 9.64	-
BC	0.52	0.37	-	0.56	0.75 – 0.91	-

G. R. van der Werf acknowledged, via personal communication, that Akagi et al., 2011 emission factors were not yet released (and thus unavailable) for use in version 3 of GFED, but will most likely be used for the development of GFED, version 4 later this year.

We feel that it is out of the scope of this manuscript to re-conduct our simulations using emission factors from Akagi et al. (2011). First, as shown above, the emission factors were not considerably different from the ones we used. Second, since these simulations were conducted using CESM with an interactive slab ocean, they were computationally intensive and would require us to identify new computer resources. Third (and most importantly), our optimization approach is unlikely to be sensitive to our initial set of aerosol emissions. Specifically, modifying the emission factors would yield new scale factors in Table 2 when compared to MISR and MODIS AOD observations, but would not likely significantly change the adjusted optical depths and thus climate forcing.

Also as is evident in van der Werf et al., 2010, building a new time series of emissions would be a challenging and time-consuming task since each grid cell would have to be partitioned into the vegetation types specified by Akagi. The scope of this manuscript was to use an existing fire emissions dataset, which had been carefully constructed, and to then assess the simulated climate response to fire

aerosol loading. It is certainly worthwhile to investigate this question in the future using GFED4 with Akagi et al., 2011 emission factors. To reflect this, we have acknowledged Akagi et al., 2011 in the text on page 28076:

[...] Aerosol emissions are then estimated using emissions factors for different biomes, drawing upon published emission factors from Andreae and Merlet (2001) that are updated annually. Akagi et al. (2011) have published an update to emission factors from Andreae and Merlet (2001) that were not available during the construction of GFEDv3, but likely will be incorporated in the future version of the GFED model [...]

3) p. 28076, line 21: How do you handle the spatial scale difference in GFEDv3 (0.5 x 0.5, monthly) and the climate drivers (0.75 x 0.75, monthly) for model simulation?

We used linear interpolation to re-grid the GFED data to model resolution (1.9 x 2.5 degrees, fv) for input files, paying careful attention to regrid the fluxes per square-meter and then apply the new fluxes to the new grid areas. We recognize that this is not clear in the paper, and have amended the text on page 28077 (lines 1-2) to now read:

Therefore, our initial simulations were forced with 2 x GFEDv3 BC and OC emissions and 1 x GFEDv3 SO₂ emissions. Initialization datasets were produced using linear interpolation to re-grid the original GFEDv3 data (0.5° x 0.5° spatial resolution) to the CAM5 resolution (1.9° x 2.5°).

4) P. 28076, line 28: Explain why GFEDv3 smoke emissions were underestimated by a factor of 2 which is very significant.

First, a small caveat – our simulations showed that using GFEDv3 emissions, CAM5-simulated aerosol optical depths were underestimated by a factor of 2-4. This is not exactly equivalent to saying that GFEDv3 smoke emissions were underestimated. Nevertheless, we do acknowledge that the absence of secondary aerosol parameterization in the model may account for some of the low bias (we discussed this on page 28077). We also acknowledge that GFEDv3 emissions estimates may have a low bias. Part of this may be explained by the inability of the MODIS instrument to detect very small fires. Randerson et al., 2012 suggest that small fires may account for up to 35% more global carbon emissions from fire over the original GFEDv3 estimates.

Furthermore, there is evidence that the fraction of liquid clouds in CAM5 is too high, and that this, combined with a potential high bias in wet deposition rates leads to excessive scavenging of aerosols, especially at lower altitudes (Wang et al., 2013). Furthermore, the rate at which BC aerosols age (the aerosol life cycle) is too fast, leading to excessive deposition.

The combination of all of these factors likely explains why CAM5 underestimates aerosol optical depths as compared to MODIS and MISR observations. To further clarify these points, we have amended the first paragraph on page 28077 with the following text:

[...] It is also likely that the GFEDv3 inventory underestimated emissions contributions from small fires by as much as 35% (Randerson et al., 2012). Furthermore, there is some evidence that liquid cloud fraction and wet deposition rates are too high in CAM5 and this contributed to increased wet aerosol deposition and thus low optical depth biases (Wang et al., 2013).

5) p. 28078, line 1: *What are the standard deviations of the mean scale factors?*

The standard deviations (S.D.) for the scale factors are very small, and the slopes are highly significant. For Equatorial Asia, the S.D. was 0.05, for southern Africa 0.07, for South America 0.07 and for Boreal North America 0.09. Because the slopes were highly significant, we chose not to include the standard deviations in the text.

6) p. 28097, Table 1: *Why is the MODIS scalar much higher than the MISR scalar for most of the regions?*

Each regional scalar is calculated (as described in the text) as the linear slope between the observed and simulated data for each region for only those months that cumulatively contribute 80% of each region's fire emissions. Thus, the larger MODIS scalars suggests that the satellite optical depths from this instrument were higher than comparable retrievals from MISR. In other words, MODIS data had a slight high bias against MISR data in each region. MISR and MODIS have different retrieval algorithms that have to varying sampling abilities over different surface types. For example, it is well known that MODIS has difficulty making aerosol retrievals over bright desert regions. These sampling discrepancies may be to blame for part of the scalar differences.

In equatorial Asia, however, the MODIS and MISR scalars were fairly similar, suggesting that observations had a similar magnitude.

7) p. 28097, Table 1: *Why are AERONET dataset not used for scaling GFEDv3 emissions?*

We used MISR and MODIS because of their continuous spatial coverage in key tropical regions where biomass burning emissions were high, and held AERONET observations in reserve for validation. MISR and MODIS provided fairly complete data for whole regions of interest which allowed for more point-to-point comparisons. In contrast, AERONET data was only available at a handful of stations within regions of interest and would not have provided enough information to properly scale optical depth data and apply the resultant scalars to the entire region.

8) p. 28099, Table 3: *Are the differences between observed and modeled optical depths statistically significant?*

Table 3 presents total average optical depth for each region averaged over the entire period, both before and after the adjustment. In every case, the standard error for each value is around 10^{-2} times smaller than the AOD value, indicating that, yes, observed and modeled optical depths were statistically different, even in the adjusted cases. Nevertheless, our goal was not to accurately model the average optical depth for each region, but rather to accurately simulate the optical depth during fire events. There are other factors affecting optical depth (sea salt and dust suspension, etc.) that were beyond our control and the scope of this experiment.

9) p. 28102, Fig. 2, *add r2 to the figures.*

10) p. 28103, Fig. 3, *add r2 and slopes to the figures.*

11) p. 28105, Fig. 5, *Label (a), (b), (c) and (d) to each figure.*

We have incorporated these changes. Instead of including r-squared values in Figs. 1 and 2, we added them to the captions to keep the figures from appearing too cluttered.

Global impact of smoke aerosols from landscape fires on climate and the Hadley circulation

M. G. Tosca^{1,2}, J. T. Randerson¹, and C. S. Zender¹

¹Department of Earth System Science, University of California, Irvine, 92697

²now at: NASA Jet Propulsion Laboratory, California Institute of Technology, Pasadena, 91109

Correspondence to: Michael G. Tosca (michael.g.tosca@jpl.nasa.gov)

Abstract. Each year landscape fires across the globe emit black and organic carbon smoke particles that can last in the atmosphere for days to weeks. We characterized the climate response to these aerosols using an Earth system model. We used remote sensing observations of aerosol optical depth (AOD) and simulations from the Community Atmosphere Model, version 5 (CAM5) to optimize satellite-derived smoke emissions for high biomass burning regions. Subsequent global simulations using the adjusted fire emissions produced AODs that were in closer agreement with surface and space-based measurements. We then used CAM5, which included radiative aerosol effects, to evaluate the climate response to the fire-aerosol forcing. We conducted two 52 year simulations, one with four sets of monthly cycling 1997-2009 fire emissions and one without. Fire emissions increased global annual mean AOD by 10% (+0.02) and decreased net all-sky surface radiation by 1% (1.3 W m⁻²). Elevated AODs reduced global surface temperatures by 0.13±0.01°C. Though global precipitation declined only slightly, patterns of precipitation changed, with large reductions near the equator offset by smaller increases north and south of the intertropical convergence zone (ITCZ). A combination of increased tropospheric heating and reduced surface temperatures increased equatorial subsidence and weakened the Hadley circulation. As a consequence, precipitation decreased over tropical forests in South America, Africa and equatorial Asia. These results are consistent with the observed correlation between global temperatures and the strength of the Hadley circulation and studies linking tropospheric heating from black carbon aerosols with tropical expansion.

Key Words: Multi-angle Imaging SpectroRadiometer (MISR), Community Earth System Model (CESM), MODerate resolution Imaging Spectroradiometer (MODIS), global carbon cycle, mean meridional circulation, biomass burning, and radiative forcing.

1 Introduction

Climate is a primary driver of global and regional fire activity, and fires, in turn, influence climate on similar temporal and spatial scales by means of emissions of trace gases and aerosols and by modifying vegetation composition and structure (Marlon et al., 2008; Power et al., 2008; Bowman et al., 2009; Ward et al., 2012). Fire incidence was low outside of the tropics and subtropics during the last glacial maximum, coinciding with cool temperatures, but increased as global temperatures began rising around 12,000 years ago (Power et al., 2008). During the last two millennia, fires decreased between AD 1 and 1750, during a period of gradual global cooling (Marlon et al., 2008). Subsequently, between 1750 and 1870, fire activity, inferred from charcoal records, rapidly increased, coinciding with a period of temperature increases but also when humans began exerting greater control on ecosystem processes through land management (Marlon et al., 2008). In the American Southwest, regionally large fire years over the last several centuries often followed dry winters preceded by several years of cool and wet conditions that allowed fuels to accumulate (Swetnam and Betancourt, 1998). In western North America, anthropogenic climate warming over the last several decades has increased the number of large wildland fires (Westerling et al., 2006) and also may have influenced burn severity and levels of fuel consumption (Turetsky et al., 2011). On interannual timescales, satellite observations of burned area and active fire thermal anomalies provide evidence that the El Niño-Southern Oscillation and other climate modes modify fire activity considerably in tropical forest and savanna ecosystems (Spessa et al., 2005; van der Werf et al., 2008; Field et al., 2009; Fernandes et al., 2011; Chen et al., 2011).

Feedbacks between climate and fires are possible because fires also modify climate through several different pathways. Fires have contributed to the accumulation of carbon dioxide and methane in the atmosphere in recent decades, for example, by enabling more rapid rates of land clearing in forest ecosystems (Crutzen et al., 1979; Langenfelds et al., 2002; Page et al., 2002). Fire emissions from **deforestation fires** were approximately **490 Tg C yr⁻¹** during 1997-2009 (van der Werf et al., 2010). This flux, **which equals a quarter of all global fire emissions** represents a net source of CO₂ because many forests are being permanently replaced by pastures and croplands. Fires also contributed to tropical forest degradation during this period (i.e. the loss of trees and biomass in nearby forests not intentionally cleared), and although this flux is difficult to quantify, it likely represents another important source of carbon emissions (Morton et al., 2011). Fires also influence climate by inducing vegetation mortality, with longer-term effects on surface albedo and energy exchange as a consequence of post-fire vegetation succession (Myhre et al., 2005; Lyons et al., 2008; Liu and Randerson, 2008). Emissions of ozone precursors may have immediate consequences for radiative forcing (Ward et al., 2012) and also longer term effects on canopy conductance and ecosystem carbon storage (Sitch et al., 2007).

In this study, we focus on another important climate driver: emissions of smoke aerosols. While the radiative effects of smoke aerosols from fires have been investigated for several decades (Kauf-

60 man et al., 1991; Penner et al., 1992; Chylek and Wong, 1995; Hansen et al., 1997; Ramanathan and
Carmichael, 2008), as described below, important uncertainties remain with respect to the temporal
and spatial magnitude of surface and top-of-atmosphere forcing caused by smoke from landscape
fires (Reid et al., 2009). Even less is known about how this forcing subsequently modifies atmo-
sphere and surface energy fluxes, cloud lifetimes, circulation characteristics, and regional to global
65 scale temperature and precipitation patterns. Here we investigate the relationship between forcing
and climate response for fires using a global Earth system model that includes direct and semi-direct
aerosol effects. In the remainder of the introduction we review recent work on smoke aerosol radi-
ative forcing and relevant processes influencing large-scale climate interactions.

Black and organic carbon (BC and OC) are primary constituents of smoke aerosols from land-
70 scape fires, with BC accounting for 5-10% of the total particle mass and OC accounting for much of
the remainder (Andreae and Merlet, 2001; Reid et al., 2005). Mahowald et al. (2011) estimate that
approximately 60 Tg of smoke is emitted from landscape fires each year. This constitutes 30% of
the total black and organic smoke mass emitted globally each year (Lamarque et al., 2010). These
aerosols alter the climate through the scattering and absorption of solar radiation, which simulta-
75 neously cools the surface and warms the atmospheric column (Penner et al., 1992; Hansen et al.,
1997; Ramanathan and Carmichael, 2008) and by modifying cloud properties (Penner et al., 1992;
Ackerman et al., 2000). Bauer and Menon (2012) estimate that the direct radiative effect of smoke
from grass fires, forest fires and agricultural waste burning is close to zero globally. This forcing,
however, is the residual of larger regional and seasonal warming and cooling terms, with negative
80 fluxes in tropical land and ocean regions and positive fluxes in polar regions. Jones et al. (2007) es-
timated the direct global radiative forcing from fire aerosols to be -0.29 W m^{-2} , leading to a global
mean temperature decrease of 0.25°C in the Hadley Centre model and a forcing efficacy of 0.86.

Accumulating evidence suggests that smoke-induced changes in net column shortwave radiation
and interactions between smoke particles and cloud droplets can modify precipitation (Andreae et al.,
85 2004; Rosenfeld, 2006; Rosenfeld et al., 2008; Andreae and Rosenfeld, 2008). Widespread convec-
tion suppression, the result of lowered surface temperatures and elevated atmospheric heating via
BC absorption increases vertical stratification which inhibits both cloud formation and precipita-
tion (Ackerman et al., 2000; Feingold et al., 2001; Tosca et al., 2010). Including smoke in climate
simulations over the Amazon caused a change in monsoonal circulation in regions with aerosol
90 optical depths greater than 0.3 (Zhang et al., 2009). In the Zhang et al. (2009) study, smoke heat-
ing increased surface pressure, decreased upward vertical velocity and reduced the lapse rate, the
combination of which increased surface divergence. As a consequence, the onset of early autumn
monsoonal rains was delayed. Analysis of satellite observations by Koren et al. (2004) provides
support for this mechanism: areas with thick smoke over the Amazon had fewer clouds. The en-
95 trainment of microscopic smoke particles into clouds also acts to suppress precipitation by slowing
the conversion of cloud drops into raindrops (Gunn and Phillips, 1957; Rosenfeld et al., 2008). Us-

ing satellite observations from the Tropical Rainfall Measuring Mission (TRMM) of smoke-polluted clouds over the Amazon, Rosenfeld (1999) detected ample water for rainfall, but a lack of precipitation due to numerous small water droplets. In contrast to the semi-direct aerosol effect described by Ackerman et al. (2000), where smoke-induced radiative heating limits the formation of trade cumulus clouds, Albrecht (1989) provided evidence that aerosols in marine stratocumulus regions increase cloudiness and decrease cloud droplet sizes, effectively limiting drizzle. Considering all of these effects together, contemporary aerosols, including smoke from landscape fires, likely weaken the hydrologic cycle (Ramanathan et al., 2001). Recent increases in tropical aerosols over the last half century from anthropogenic activity (Field et al., 2009) may offset the expected strengthening of the hydrologic cycle from global warming (Held and Soden, 2006).

In some areas, ingestion of smoke aerosols into ice-phase cumulonimbus clouds may increase local precipitation. In smoke-polluted cumulus clouds, the percentage of droplets above the freezing level is larger, which maximizes the lifetime and vertical size of the cloud and increases the intensity of downdrafts and precipitation rates (Rosenfeld et al., 2008). Koren et al. (2005) observed invigoration of convective clouds by biomass burning aerosols over the Atlantic Ocean. Taken together, these studies illustrate the uncertainties involved in understanding fire aerosol effects at the global scale. However, the inclusion of improved moist turbulence schemes and better representation of aerosol-cloud microphysical interactions in Earth system models (Bretherton and Park, 2009) provide unique opportunities to examine fire aerosol effects on regional and global climate.

Recent work suggests that the mean strength of the Hadley circulation is increasing (Mitas and Clement, 2005), and though most attribute this strengthening and expansion to higher surface temperatures (Lu et al., 2007; Quan et al., 2005), there is evidence that aerosols, especially black carbon and sulfate, play a role in altering the mean circulation (Yoshimori and Broccoli, 2009). Jones et al. (2007) suggest that increased atmospheric loading of biomass burning aerosols shifts the location of the inter-tropical convergence zone, and Allen et al. (2012b) argue that black carbon aerosol forcing helps explain the seasonality and extent of recent Hadley cell expansion. Specifically, black carbon-induced heating of the lower troposphere at mid-latitudes significantly contributes to the observed poleward shift of the descending branch of the Hadley circulation (Allen et al., 2012a,b). Our work isolates the impact of fire aerosols on mean global circulation patterns using an Earth system model that includes direct and semi-direct aerosol effects. In addition, we quantify the impact of smoke aerosols on climate variables intrinsically linked to precipitation and radiation changes.

2 Methods

We used an Earth system model with interactive atmospheric chemistry to simulate climate with and without landscape fire aerosols. We first optimized black carbon (BC) and organic carbon (OC) emissions from fire by matching simulated aerosol optical depths (AODs) to observations and scaling

emissions by regionally unique factors that best matched observed AODs in high biomass burning regions. We then performed two 52-year simulations with and without the adjusted fire aerosol emissions and assessed the impact of these aerosols on global temperature, precipitation and the mean Hadley circulation.

2.1 Model and data description

For our simulations we used the Community Earth System Model (CESM), version 1 initialized with the Community Atmosphere Model, version 5 (CAM5), and the single-layer ocean model (SOM) (Neale et al., 2010). The full chemistry model embedded in CAM5 for this experiment was the Model for Ozone and Related Chemical Tracers, version 4 (MOZART-4) (Emmons et al., 2010). Like previous versions of CAM (CAM3 and CAM4), this configuration (trop_mozart) includes direct and semi-direct aerosol radiative effects (Collins et al., 2004) and utilizes the bulk aerosol model (BAM) configuration (Rasch et al., 2001; Lamarque et al., 2012). The moist turbulence scheme in CAM5 replaces the dry turbulence scheme in previous versions and explicitly simulates cloud-radiation-turbulence interactions allowing for a more realistic simulation of aerosol semi-direct effects in stratus clouds (Bretherton and Park, 2009). Also included in CAM5 are an improved shallow convection scheme and a revised cloud macrophysics scheme (Neale et al., 2010). The atmospheric chemistry component is now fully interactive and embedded within CAM5 and handles emissions of aerosols and trace gases and deposition of aerosols to snow, ice and vegetation. Our simulations did not use the Modal Aerosol Model (MAM) to simulate cloud indirect effects (Liu et al., 2012) with efforts still ongoing to improve the representation of these processes within CAM. Evaluating indirect effects on the climate response documented here is an important next step.

To estimate landscape fire emissions, we used gaseous and particulate fire emissions from the Global Fire Emissions Database, version 3 (GFEDv3) (van der Werf et al., 2010). Calculation of burned area in GFEDv3 is described by Giglio et al. (2010). Fuel loads and combustion completeness factors are estimated using a biogeochemical model and are combined with satellite-derived burned area estimates to derive total carbon emissions. Aerosol emissions are then estimated from total emissions using emissions factors for different biomes, drawing upon published emission factors from Andreae and Merlet (2001) that are updated annually. **Akagi et al. (2011) have published an update to emission factors from Andreae and Merlet (2001) that were not available during the construction of GFEDv3, but likely will be incorporated in future version of the GFED model.** We used the Multi-angle Imaging SpectroRadiometer (MISR) Level 3 daily AOD product (MIL3MAE) and the Moderate Resolution Imaging Spectro-radiometer (MODIS) Level 3, Collection 5 monthly AOD product (MOD08 M3) to assist in scaling the GFED aerosol emissions.

We used ground-based Aerosol Robotic Network (AERONET) optical depth data (Holben et al., 1998) from 21 individual stations to evaluate our model simulations with adjusted emissions. We assessed the strength and spatial location of the Hadley circulation using horizontal and vertical wind

170 velocities obtained from the European Centre for Medium-Range Weather Forecasting (ECMWF) interim Reanalysis product (ERA-interim) (Dee et al., 2011). Monthly ERA-interim data were available from 1989-2011 at a $0.75^\circ \times 0.75^\circ$ horizontal resolution with 60 vertical levels.

2.2 Scaling fire emissions to achieve realistic AODs

We forced an initial simulation of the CAM5-SOM configuration of CESM with monthly varying fire emissions from GFEDv3 during 1997-2009. Evidence from Ward et al. (2012) suggests that to accurately simulate observed aerosol optical depths, GFEDv3 smoke emissions need to be approximately 175 doubled. Therefore, our initial simulations were forced with $2 \times$ GFEDv3 BC and OC emissions and $1 \times$ GFEDv3 SO_2 emissions. **Initialization datasets were produced using linear interpolation to re-grid the original GFEDv3 data ($0.5^\circ \times 0.5^\circ$ spatial resolution) to the CAM5 resolution ($1.9^\circ \times 2.5^\circ$).** This study isolated the climate response to aerosols-only; we thus excluded altering nitrogen emissions as some molecules of NO_2 act as precursors to ozone formation. Aerosols were injected 180 into the lowest layer of the model, as evidence suggests that smoke injection above the boundary layer is rare (Martin et al., 2010; Tosca et al., 2011).

Comparison of the resulting CAM5-simulated AODs to observations from both MISR and MODIS revealed a low bias in biomass burning regions (Figure S1). Some of the bias may be explained a lack of an explicit parametrization of secondary aerosol condensation and coagulation 185 processes in CAM5. Specifically, the emission factors we used from Andreae and Merlet (2001) may include measurements made prior to significant plume aging and condensation. Studies have shown that secondary aerosols constitute a significant fraction of the total aerosol mass within biomass burning plumes (Lee et al., 2008; Grieshop et al., 2009). For example, organic carbon aerosol concentrations increased by factors of 1.5 to 6 after 3 to 4 hours of aging downwind of a prescribed fire 190 in Georgia (Lee et al., 2008). It is also likely that the GFEDv3 inventory underestimated emissions contributions from small fires **by as much as 35% (Randerson et al., 2012). Furthermore, there is some evidence that liquid cloud fraction and wet deposition rates are too high in CAM5 and this contributed to increased wet aerosol deposition and thus low optical depth biases (Wang et al., 2013).**

195 In the three major tropical burning regions of South America (SAM), southern Africa (SAF) and equatorial Asia (EAS) (Figure 1), AODs were substantially lower than observations from MISR and MODIS (Figure 2). For these regions, and also for boreal North America, we computed the scaling factor required to bring the AODs into agreement with the satellite time series. Our scaling factors apply only to direct aerosols emissions as we did not explicitly include any parametrization of 200 secondary organic aerosol formation within fire plumes. We chose regions where fire aerosols were the dominant contributor to the optical depth signal within CAM5, thereby increasing the likelihood of a monotonic relation between emissions and optical depth (Figure S2). We chose SAM (25°S - 0° ; 65°W - 40°W), SAF (15°S - 5°S ; 10°E - 30°E), EAS (10°S - 7°N ; 90°E - 150°E) and boreal North

America (BNA; 50°N-70 °N; 170°W-90°W) as our initial scaling regions. We then derived four
205 regionally-specific mean scale factors by computing the ordinary least squares regression between
the simulated AOD (independent variable) and the observed (dependent variable) for those months
in the time series that cumulatively contributed to 80% of regional fire emissions (Table 1). Each
region's mean scaling factor was the average of scalars derived separately for MISR and MODIS
observations. In other regions, where contributions from other aerosol sources were proportionally
210 larger, it was not possible to use this optimization approach. In these regions we assigned scale
factors based on ecosystem similarity and proximity. The scalars for SA, SAF, EAS and BNA were
2.40, 2.10, 1.67 and 1.45, respectively, and were applied to biogeographically similar regions as
shown in Table 2. In a second simulation we increased emissions by these scalars, preserving the
same spatial and temporal distributions. Global smoke (the sum of BC and OC) emissions from
215 landscape fires increased from 40.6 Tg yr⁻¹ to 79.9 Tg yr⁻¹, as a result of the adjustment process.
Total SO₂ emissions were adjusted upward from 2.4 to 4.7 Tg yr⁻¹. These adjustments were broadly
similar to estimates from Johnston et al. (2012) who applied similar scaling techniques using the
global GEOS-Chem model to study aerosol effects on human health. Time series biases, root mean
squared errors and linear correlations (slopes) for each region showed considerable improvement
220 between the original and adjusted cases (Figure S3).

The second simulation, using adjusted emissions, produced linear fits between modeled and
satellite-observed AODs that had slopes closer to 1.0 (ranging from 0.72 to 0.87 for SA, SAF, EAS;
Figure 2). We evaluated our adjustments using AOD data from 21 individual AERONET stations
across the tropics (Figure 1). This confirmed our initial assumption that the relation between AODs
225 and emissions was mostly linear. We compared CAM5 simulated optical depth to observations for
only those months when greater than 30% of the optical depth from CAM5 was derived from fire.
Even after **considering the large spatial-scale mismatches** between the model and the observations,
our analysis revealed significant improvement in the linear relation between modeled and observed
optical depths for individual stations in SA, SAF and EAS (Figure 3). Despite general improve-
230 ment between the original and adjusted cases, low-biases still persisted in eastern Africa and parts of
equatorial Asia. This suggests the climate impacts we describe in the following sections are likely to
be conservative. Table 3 summarizes the AOD improvements for the simulations we obtained after
optimization.

2.3 Effects of fire aerosols on climate using CESM

235 We used the same configuration of CAM5-SOM (described in Section 2.1) to investigate the simu-
lated climate response to fire aerosol forcing. We conducted two simulations: one with no prescribed
surface fire aerosol emissions (NOFIRE), but aerosols emissions from all other sources, and one with
surface fire aerosol emissions (FIRE) in addition to all other aerosol sources. Emissions for most
species were compiled and adapted from various sources into a comprehensive data set described

240 by Lamarque et al. (2010). More specifically, surface emissions of trace gases and aerosols from industrial and natural non-fire sources were based on MOZART-4 emissions described in Emmons et al. (2010). For most species, anthropogenic emissions were from the POET inventory (Granier et al., 2005), except in Asia where emissions from the REAS inventory were substituted (Ohara et al., 2007). Fire emissions of BC, OC and SO₂ were obtained following the approach described in
245 Section 2.2 (above). Fire emissions of other minor aerosols and trace gases were prescribed directly from GFEDv3. The standard configuration of the Community Land Model (CLM) automatically quantifies the radiative forcing associated with black carbon deposition on snow, which proves consequential to the high latitude climate response.

Each simulation began after a 15-year spin-up period and lasted for 52 years. For the FIRE case we forced the model with four cycles of the adjusted 1997-2009 emissions described above. As a result, the FIRE simulation included observed year-to-year variability in emissions during each cycle. The NOFIRE simulation was identical to the FIRE simulation but did not include fire emissions of OC, BC or SO₂. The use of 52 year simulations allowed us to quantify fire-induced climate responses in a statistically robust way given the internal climate variability within each simulation and also the large interannual variability of fire emissions that occurred in many regions.

250
255

3 Results

3.1 Spatial and meridional climate response to fire aerosol emissions

The presence of fire aerosols in the FIRE simulation produced a global, area-weighted AOD increase of $1.5 \times 10^{-2} \pm 0.2 \times 10^{-2}$ (10%) (Table 4), and large regional increases over the middle of central South America, Africa and equatorial Asia (Figure 4). Remote swaths of open ocean also exhibited significant AOD increases (between 0.001 and 0.01), suggesting that the lifetimes of some fire aerosols were long enough to allow for long-range transport. In most cases, the maximum AOD increases occurred over regions of consistently high fire emissions. For example, over southern Africa (15°S-5°S; 10°E-30°E) and South America (25°S-0; 65°E-50°E) fires increased annual mean AOD by an area-averaged 0.19 ± 0.03 (199%) and 0.08 ± 0.02 (91%), respectively. Zonally averaged global AOD increases were at a maximum of 0.06 between 10°S and 10°N, corresponding to consistently high fire emissions over Africa and South America, with another relative maximum between 50°N and 60°N over North American and Eurasian boreal forests (Figure 5). Optical depth
265
270 exhibited a clear seasonal cycle and reached a zonally-averaged maximum during DJF around 5°N (0.11) and during JJA at 5°S (0.10).

The total, top of atmosphere, direct radiative forcing from fire aerosols was $+0.18 \pm 0.10 \text{ W m}^{-2}$ (Figure 6a; Table 4). Regions of highest positive radiative forcing were generally in the tropical oceans, corresponding to high AODs, though directly over fire source regions (e.g. central Ama-

275 zonia, boreal North America), radiative forcing was slightly negative. In response to the aerosol
forcing, globally averaged all-sky net surface shortwave (S_{net}) decreased by $1.3 \pm 0.2 \text{ W m}^{-2}$ (1%;
Figure 6b; Table 4). Like AOD, the largest changes occurred near or downwind of the major tropical
burning regions. Area-averaged decreases over southern Africa (for the same region defined above)
and South America (for the same region defined above) were $-19.1 \pm 3.2 \text{ W m}^{-2}$ (8%) and $-9.1 \pm$
280 1.8 W m^{-2} (4%), respectively, with negative anomalies up to -30 W m^{-2} over some regions within
southern Africa. The zonally averaged pattern of S_{net} anomalies closely followed AOD, with the
maximum reduction (-5 W m^{-2}) occurring just south of the equator (Figure 5).

The combination of increased AOD and reduced surface shortwave radiation reduced surface tem-
perature in most areas ($0.13 \pm 0.01^\circ\text{C}$, Table 4, Figure 6c). Outside of the intertropical convergence
285 zone (ITCZ) in the eastern Pacific and the high-latitude storm tracks, the largest reductions in tem-
perature occurred over the continents. In southern Africa (same region as above) average temper-
ature decreased by $0.46 \pm 0.07^\circ\text{C}$, and over the southern Amazon (same region as above) by 0.37
 $\pm 0.07^\circ\text{C}$. Global temperature anomalies were at a zonally-averaged minimum at the equator and
northward (-0.2°C) but large reductions also occurred near the South pole. Temperatures decreases
290 near the equator and 60°N corresponded with a relatively smaller zonal AOD maximum, suggesting
that direct forcing from aerosols at higher latitudes had a proportionately greater impact. However,
the lack of a significant spatial correlation between temperature changes and S_{net} anomalies sug-
gests that direct effects from smoke on the local atmosphere and surface radiation budget were not
responsible for all of the meridional and global temperature response.

295 On average, global precipitation decreased $2.9 \times 10^{-2} \pm 0.3 \times 10^{-2} \text{ mm d}^{-1}$ (1%) (Table 4), but
anomalies showed a complex spatial pattern of large precipitation decreases at the equator, slightly
smaller decreases in the Northern Hemisphere storm track and increases between 5 and 10°N (and
 5 and 10°S). Over the main burning regions of Africa and South America, precipitation decreased
 $2.4 \times 10^{-1} \pm 0.5 \times 10^{-1} \text{ mm d}^{-1}$ (7%) and $0.8 \times 10^{-1} \pm 0.5 \times 10^{-1} \text{ mm d}^{-1}$ (2%), respectively.
300 Some of this precipitation decrease appeared to have been caused by local aerosol effects on surface
convergence, upward vertical wind speeds (ω) and atmospheric warming and its effect on the lapse
rate. For example, the temperature difference over Africa (same region as above) between 700mb
and the surface decreased by $0.43 \pm 0.10^\circ\text{C}$, reflecting increased atmospheric stability and occurring
simultaneously with a decrease in upward wind velocity of $9.1 \times 10^{-4} \pm 12.7 \times 10^{-4} \text{ Pa s}^{-1}$ at 500mb
305 (Figure S4). It is likely, however, that other mechanisms are needed to explain the macroscale change
in global precipitation, including changes in the remote Pacific shown in Figure 4d.

3.2 Fire aerosol effects on the Hadley Circulation

We used meridional wind velocities and surface pressure to compute the annual mean mass stream-
function (described by Oort and Yienger (1996)) for ERA-interim data and our CAM5 simulations
310 (Figure 7a,b). Two Hadley cells, between 30°S and 30°N were visible in both the ERA-interim data

as well as the CAM5 simulations. The model adequately matched the placement and strength of the two cells when compared to the reanalysis. The simulated and observed streamfunctions (ψ) placed the dividing line between the southern and northern Hadley cells just north of the equator, corresponding to the latitude of mean ascent and near-permanent residence of the ITCZ at 5°N. ERA-interim data indicated a slightly stronger southern Hadley cell with maximum ψ values exceeding $-11 \times 10^{10} \text{ kg s}^{-1}$, compared to $-8.5 \times 10^{10} \text{ kg s}^{-1}$ for CAM5. However, maximum ψ values for the northern cell were similar between model and data: $8.1 \times 10^{10} \text{ kg s}^{-1}$ vs. $8.8 \times 10^{10} \text{ kg s}^{-1}$, respectively. Vertical velocity (ω) fields from ERA-interim data and CAM5 simulations showed the region of maximum ascent (negative ω values) between 10°S and 10°N, roughly corresponding to the division between the northern and southern Hadley cells (Figure 8a, b). Upward velocities near $2 \times 10^{-2} \text{ m s}^{-1}$ characterized the ascending branches of the Hadley cells.

Presence of fire aerosols at the equator in the FIRE simulation weakened both the northern and southern Hadley cells (Figure 7c,d). The southern Hadley cell increased by as much as $3.0 \times 10^9 \text{ kg s}^{-1}$ around 5°S, representing a net reduction in southward transport of around 10%, though reductions were smaller further south in the region of maximum absolute ψ . Similarly, ψ values in the northern Hadley cell decreased by $-3.8 \times 10^9 \text{ kg s}^{-1}$ at 5°N, also an approximate 10% reduction in northward transport. The maximum ψ for DJF decreased from 2.30×10^{11} to $2.27 \times 10^{11} \text{ kg s}^{-1}$ (a reduction of $0.3 \pm 0.2 \times 10^{10} \text{ kg s}^{-1}$), though reductions in excess of $6.7 \times 10^9 \text{ kg s}^{-1}$ occurred closer to the equator. Despite Hadley cell weakening, the width of the tropics increased slightly. We calculated the annually averaged northward extent of the Hadley cell for each simulation as the latitude (ϕ) at which ψ (at 500mb) switched from positive to negative as described in Allen et al. (2012a). We found that $\Delta\phi$ between the FIRE and NOFIRE cases was $0.4 \pm 0.4^\circ$ suggesting that the tropics widened.

Weakening of the Hadley circulation was likely a result of the aerosol forcing between 10°S and 10°N (e.g. Figure 7d). Elevated fire aerosols in this latitude band both cooled the surface and warmed the atmosphere. In some places, local aerosol-induced subsidence (more positive values of ω) contributed to the reduction in ψ values near the equator. For example, during the northern hemisphere summer (May-October), high AODs over southern Africa contributed to a column heating of greater than 0.9 K d^{-1} from 1000-700 mb and local maximum temperature increase of 0.4°C at 700mb, both of which increased ω by $4 \times 10^{-2} \text{ Pa s}^{-1}$ near 850mb and limited the amount of equatorial convection (Figure S5). This caused a local weakening of the poleward transport of mass in the southern Hadley cell.

Similarly, the global reduction in upward vertical velocities near the equator (and subsequent weakening of ψ , Figure 8c) appeared to be linked with sharp reductions in SST and mid-tropospheric heating in a narrow swath between 5°S and 5°N. In particular, over much of the Pacific the largest ω increases were co-located with reductions in SSTs, suggesting that the fire-induced temperature decreases had the largest effect on ω in regions of maximum convection. Pronounced heating be-

tween 1000 and 500 mb suggested that the long-range transport of aerosols over the Pacific contributed to the suppression of convection. Sharp decreases in atmospheric heating rates at altitudes
350 above 500mb corroborate a reduction in mid to upper level condensation. Over the tropical Pacific (180°W-90°W), ω anomalies exceeded $2.0 \times 10^{-5} \text{ Pa s}^{-1}$ in response to SST reductions greater than 0.3°C and maximum heating rates of 0.1 K d^{-1} at 850 mb (Figure S6).

4 Discussion

Simulated fire aerosols reduced net surface shortwave radiation, especially over the major burning
355 regions of South America, Africa and equatorial Asia, and increased atmospheric warming, especially in the tropics and mid-latitudes. Global surface air temperatures were lower and in some places negative anomalies exceeded -0.5°C . Though changes in surface radiation were largely confined to high biomass burning regions, the temperature response was more globally distributed. This was likely due to a substantial reduction in heat transport from the tropics to mid and high latitude
360 regions. The surface temperature reductions combined with increased tropospheric heating near the equator reduced convection in the ascending branches of the two Hadley cells. These results were consistent with conclusions from Tosca et al. (2010) that showed a link between fire emissions and precipitation reductions in equatorial Asia. In sum, the presence of fire aerosols in the troposphere caused a small general weakening of the northern and southern Hadley cells in simulations with
365 CAM5.

The mechanisms for Hadley cell weakening are also largely consistent with results from Quan et al. (2005) that link SSTs to the strength of the Hadley circulation. They suggest that from 1950 to present, increased surface temperatures have contributed to a gradual strengthening of the Hadley circulation. They also note that the strength of the Hadley circulation is positively correlated with El
370 Niño (warm SST) events in the eastern Pacific (and negatively correlated with La Niña [cold SST] events). Mitas and Clement (2005) and Lu et al. (2007) also present evidence that surface warming is positively correlated with Hadley cell strength.

The latter study found a $50.4 \times 10^8 \text{ kg s}^{-1}$ increase in the maximum DJF northern hemisphere mass streamfunction during 1979-2003, a period when surface temperatures increased by 0.6°C
375 (Hansen et al., 2010). Given a mean value of $8.8 \times 10^{10} \text{ kg s}^{-1}$, this corresponds to a cumulative increase of 5.7%. Although decadal changes in fire emissions are not well understood, it is likely that deforestation and savanna woodland fires have increased significantly since 1950. For illustrative purposes, if we assume fires increased by approximately 50% over this time, then, **using a preliminary analysis of output from our simulations**, fires may have offset Hadley strengthening
380 during this interval by $4 \times 10^8 \text{ kg s}^{-1}$. Thus, in the absence of possible changes in the fire regime, the strengthening of the Hadley circulation could have been approximately 8% greater.

Analysis of reanalysis observations suggest that the width of the Northern Hemisphere Hadley

circulation has increased in recent decades, by $0.3^\circ/\text{decade}$ during 1979–1999 (Allen et al., 2012a). Though we simulate a decrease in Hadley cell strength, we also show a significant widening of the annual northern Hadley cell ($\Delta\phi = 0.4 \pm 0.4^\circ$), in the same direction as the observations. This is consistent with results from Allen et al. (2012b) who show that recent observations of Hadley cell expansion can be partly attributed to midlatitude tropospheric heating from black carbon aerosols. Using various measures for determining tropical width, their simulations attribute **an increase of** $0.3\text{--}1.0^\circ/\text{decade}$ for 1979–2009 from midlatitude BC warming of the lower troposphere. Surface air warming from greenhouse gas forcing is known to partially explain recent increases in Hadley cell strength, but a stronger Hadley circulation usually results in an equatorward contraction (Lu et al., 2008). However, black carbon heating increases atmospheric stability which pushes the baroclinic zone poleward, resulting in an expansion of the Hadley cell. Following the same fire scenario as in the previous paragraph, our CESM simulations suggest fires may have contributed **to approximately** 10% of the observed trend.

Given that we scaled fire emissions to match simulated AODs to observations in burning regions, it is likely that our simulations adequately but conservatively captured the magnitude of the direct forcing from fire aerosols. For example, we estimated that fires increased AOD by approximately 0.02 which is in line with estimates of 0.02–0.03 from Mahowald et al. (2011) and 0.03 from Bauer and Menon (2012). This represented a 10% increase over the global background aerosol load. We also acknowledge that scaling surface emissions so that simulated AODs match observations is not a seamless fix to the underestimation of AOD within CAM5, and that other factors, such as secondary aerosol formation, and wet deposition processes (Xian et al., 2009) may contribute to discrepancies between simulations and observations.

Our results demonstrate a plausible link between smoke aerosols and changes in global circulation but do not address whether simulated circulation changes have any impact on fire distribution or occurrence. Elevated AODs generally reduced surface temperatures, especially those in the tropical Pacific where our simulations showed a La Niña-like response to the smoke forcing. The combination of decreased temperatures, atmospheric heating and aerosol-cloud indirect effects reduced convection at the equator and weakened the Hadley circulation. Over some locales, like the tropical forests of Africa and South America, simulated reductions in precipitation (between 5 and 15%) lowered soil moisture content in the top several layers which increased drought stress. This would make it easier for land managers to use fire as a tool in clearing land for pastures, croplands or plantations. Combined with the modeled relationship between global warming and tropical drying (Neelin et al., 2006), the increased drought stress may enhance positive feedbacks between fire and climate. However, some of these ecosystem impacts are likely offset or modified by the strengthening of the Hadley cells in response to global warming.

Owing to the coarse resolution of CAM5 and the complicated relationship between cloud microphysics and aerosols, it is intrinsically difficult to simulate the mesoscale meteorological response to

420 smoke. In regions like equatorial Asia geography and complicated sea-breeze interactions make it difficult to model convection, and thus difficult to fully realize the climate response to smoke-aerosol forcing. We note the difficulty in accurately representing spatial and temporal patterns of precipitation and circulation changes. This study, therefore, is a first estimate of the global climate response to fire emissions from CAM5 that accounts for direct and semi-direct aerosol effects.

425 **5 Conclusions**

We used a global climate model to simulate the sensitivity of the climate to fire aerosols. We first optimized black and organic carbon emissions by matching simulated and observed optical depths. Validation of modeled AODs with surface-based measurements showed that our emissions yielded more realistic distributions of aerosols after our scaling approach. Global simulations that included 430 fire emissions produced elevated AODs, especially across the tropics. In response to the aerosol forcing, global temperatures declined with maximum reductions in the tropics. Changes in precipitation patterns suggest that fire-emitted aerosols modify global circulation through a combination of decreased surface insolation, atmospheric heating, reduced surface temperature and increased subsidence globally and in tropical convective regions. Our results suggest a link between fire aerosols 435 and the strength and extent of the Hadley circulation.

Important next steps include assessing the regional impact of fire aerosols, inclusion of indirect effects in modeling studies and determining the relative importance of the direct and indirect aerosol contributions to the climate response. Assessing which regions contribute the most to the large response in the eastern Pacific could be done by isolating emissions from Africa, South America 440 and other high burning regions in individual simulations. Furthermore, the Modal Aerosol Model (MAM) has been developed and embedded in the latest version of CAM5 and simulates aerosol indirect effects in stratus clouds (Liu et al., 2012). One important direction for future research is to isolate the individual contributions from the direct and indirect aerosol effects, using MAM embedded within CAM5. Another important next step is understanding the combined effects of 445 fire-induced changes in solar radiation, precipitation, albedo and deposition on tropical ecosystem function.

Acknowledgements. We are grateful for support from NSF (AGS-1048890) and NASA (NNX11AF96G). M.G.T. received support from a NASA Earth and Space Science Fellowship (NNX08AU90H). C.S.Z. acknowledges NSF (ARC-0714088) and NASA (NNX07AR23G) support.

450 References

- Ackerman, A. S., Toon, O. B., Stevens, D. E., Heymsfield, A. J., Ramanathan, V., and Welton, E. J.: Reduction of tropical cloudiness by soot, *Science*, 288, 1042–1047, doi:10.1126/science.288.5468.1042, 2000.
- Akagi, S. K., Yokelson, R. J., Wiedinmyer, C., Alvarado, M. J., Reid, J. S., Karl, T., Crouse, J. D., and Wennberg, P. O.: Emission factors for open and domestic biomass burning for use in atmospheric models, *Atmos. Chem. Phys.*, 11, 4039–4072, doi:10.5194/acp-11-4039-2011, 2011.
- Albrecht, B. A.: Aerosols, cloud microphysics, and fractional cloudiness, *Science*, 245, 1227–1230, 1989.
- Allen, R. J., Sherwood, S. C., Norris, J. R., and Zender, C. S.: The equilibrium response to idealized thermal forcings in a comprehensive GCM: implications for recent tropical expansion, *Atmos. Chem. Phys.*, 12, 4795–4816, doi:10.5194/acp-12-4795-2012, 2012a.
- Allen, R. J., Sherwood, S. C., Norris, J. R., and Zender, C. S.: Recent Northern Hemisphere tropical expansion primarily driven by heterogeneous warming agents, *Nature*, 485, 350–354, 2012b.
- Andreae, M. O. and Merlet, P.: Emission of trace gases and aerosols from biomass burning, *Glob. Biogeochem. Cy.*, 15, 955–966, 2001.
- Andreae, M. O. and Rosenfeld, D.: Aerosol cloud precipitation interactions. Part 1. The nature and sources of cloud-active aerosols, *Earth Sci. Rev.*, 89, 13–41, 2008.
- Andreae, M. O., Rosenfeld, D., Artaxo, P., Costa, A. A., Frank, G. P., Longo, K. M., and Silva-Dias, M. A. F.: Smoking rain clouds over the Amazon, *Science*, 303, 1337–1342, doi:10.1126/science.1092779, 2004.
- Bauer, S. E. and Menon, S.: Aerosol direct, indirect, semidirect, and surface albedo effects from sector contributions based on the IPCC AR5 emissions for preindustrial and present-day conditions, *J. Geophys. Res.*, 117, D01 206, doi:10.1029/2011JD016816, 2012.
- Bowman, D. M. J. S., Balch, J. K., Ataxo, P., Bond, W. J., Carlson, J. M., Cochrane, M. A., D’Antonio, C. M., DeFries, R. S., Doyle, J. C., Harrison, S. P., Johnston, F. H., Keeley, J. E., Krawchuk, M. A., Kull, C. A., Marston, J. B., Moritz, M. A., Prentice, I. C., Roos, C. I., Scott, A. C., Swetnam, T. W., van der Werf, G. R., and Pyne, S. J.: Fire in the Earth System, *Science*, 324, 481–484, doi:10.1126/science.1163886, 2009.
- Bretherton, C. S. and Park, S.: A new moist turbulence parametrization in the Community Atmosphere Model, *J. Clim.*, 22, 3422–3448, 2009.
- Chen, Y., Randerson, J. T., Morton, D. C., DeFries, R. S., Collatz, G. J., Kasibhatla, P. S., Giglio, L., Jin, Y., and Marlier, M. E.: Forecasting fire season severity in South America using sea surface temperature anomalies, *Science*, 334, 787–791, doi:10.1126/science.1209472, 2011.
- Chylek, P. and Wong, J.: Effect of absorbing aerosols on global radiation budget, *Geophys. Res. Lett.*, 8, 929–931, 1995.
- Collins, W. D., Rasch, P. J., Boville, A., Hack, J. J., MaCaa, J. R., Williamson, D. L., Kiehl, J. T., Briegleb, B. P., Bitz, C., Lin, S. J., Zhang, M., and Dai, Y.: Description of the NCAR Community Atmosphere Model (CAM 3.0), Tech. rep., National Center for Atmospheric Research, 2004.
- Crutzen, P. J., Heidt, L. E., Krasnec, J. P., Pollock, W. H., and Seiler, W.: Biomass burning as a source of atmospheric gases CO, H₂ N₂O, NO, CH₃Cl and COS, *Nature*, 282, 253–256, 1979.
- Dee, D. P., Uppala, S. M., Simmons, A. J., Berrisford, P., Poli, P., Kobayashi, S., Andrae, U., Balmaseda, M. A., Balsamo, G., Bauer, P., Bechtold, P., Beljaars, A. C. M., van de Berg, L., Bidlot, J., Bormann, N., Delsol, C., Dragani, R., Fuentes, M., Geer, A. J., Haimberger, L., Healy, S. B., Hersbach, H., Holm, E. V., Isaksen,

- 490 L., Kallberg, P., Kohler, M., Matricardi, M., McNally, A. P., Monge-Sanz, B. M., Morcrette, J.-J., Park, B.-K., Peubey, C., de Rosnay, P., Tavolato, C., Thepaut, J.-N., and Vitart, F.: The ERA-Interim reanalysis: configuration and performance of the data assimilation system, *Q. J. R. Meteorol. Soc.*, 137, 553–597, 2011.
- Emmons, L. K., Walters, S., Hess, P. G., Lamarque, J.-F., Pfister, G. G., Fillmore, D., Granier, C., Guenther, A., Kinnison, D., Laepple, T., Orlando, J., Tie, X., Tyndall, G., Wiedinmyer, C., Baughcum, S. L., and
495 Kloster, S.: Description and evaluation of the Model for Ozone and Related chemical Tracers, version 4 (MOZART-4), *Geosci. Model Dev.*, 3, 43–67, doi:www.geosci-model-dev.net/3/43/2010/, 2010.
- Feingold, G., Remer, L. A., Ramaprasad, J., and Kaufman, Y. J.: Analysis of smoke impact on clouds in Brazilian biomass burning regions: An extension of Twomey’s approach, *J. Geophys. Res.*, 106, 22 907–22 922, 2001.
- 500 Fernandes, K., Baethgen, W., Bernardes, S., DeFries, R., DeWitt, D. G., Goddard, L., Lavado, W., Lee, D. E., Padoch, C., Pinedo-Vasquez, M., and Uriarte, M.: North tropical Atlantic influence on western Amazon fire season variability, *Geophys. Res. Lett.*, 38, L12 701, doi:10.1029/2011GL047392, 2011.
- Field, R. D., van der Werf, G. R., and Shen, S. S. P.: Human amplification of drought-induced biomass burning in Indonesia since 1960, *Nature Geo.*, 2, 185–188, doi:10.1038/NGEO443, 2009.
- 505 Giglio, L., Randerson, J. T., van der Werf, G. R., Kasibhatla, P. S., Collatz, G. J., Morton, D. C., and DeFries, R. S.: Assessing variability and long-term trends in burned area by merging multiple satellite fire products, *Biogeosci.*, 7, 1171–1186, doi:10.1111/j.1365-2486.2009.02078.x, 2010.
- Granier, C., Lamarque, J. F., Mieville, A., Muller, J. F., Olivier, J., Orlando, J., Peters, J., Petron, G., Tyndall, G., and Wallens, S.: POET, a database of surface emissions of ozone precursors, available on the internet at:
510 <http://www.aero.jussieu.fr/projet/ACCENT/POET.php>, 2005.
- Grieshop, A. P., Logue, J. M., Donahue, N. M., and Robinson, A. L.: Laboratory investigation of photochemical oxidation of organic aerosol from wood fires 1: measurement and simulation of organic aerosol evolution, *Atmos. Chem. Phys.*, 9, 1263–1277, doi:10.5194/acp-9-1263-2009, 2009.
- Gunn, R. and Phillips, B. B.: An experimental investigation of the effect of air pollution on the initiation of
515 rain, *J. Meteor.*, 14, 272–280, doi:http://dx.doi.org/10.1175/1520-0469(1957)014<0272:AEIOTE>2.0.CO;2, 1957.
- Hansen, J., Sato, M., and Ruedy, R.: Radiative forcing and climate response, *J. Geophys. Res.*, 102, 6831–6864, 1997.
- Hansen, J., Ruedy, R., Sato, M., and Lo, K.: Global surface temperature change, *Rev. Geophys.*, 48, RG4004,
520 2010.
- Held, I. M. and Soden, B. J.: Robust responses of the hydrological cycle to global warming, *J. Clim.*, 19, 5686–5699, doi:10.1175/2010JCLI4045.1, 2006.
- Holben, B. N., Eck, T. F., Slutsker, I., Tanre, D., p. Buis, J., Setzer, A., Vermote, E., Reagan, J. A., Kaufman, Y., Makajima, T., Lavenu, F., Jankowiak, I., and Smirnov, A.: AERONET - A federated instrument network
525 and data archive for aerosol characterization, *Rem. Sense. Environ.*, 66, 1–16, 1998.
- Johnston, F. H., Henderson, S. B., Chen, Y., Randerson, J. T., Marlier, M., DeFries, R. S., Kinney, P., Bowman, D. M. J. S., and Brauer, M.: Estimated global mortality attributable to smoke from landscape fires, *Enviro. Health Per.*, 120, 695–701, doi:10.1289/ehp.1104422, 2012.
- Jones, A., Haywood, J. M., and Boucher, O.: Aerosol forcing, climate response and climate sensitivity in the

- 530 Hadley Centre climate model, *J. Geophys. Res.*, 112, D20 211, doi:10.1029/2007JD008688, 2007.
- Kaufman, Y. J., Fraser, R. S., and Mahoney, R. L.: Fossil fuel and biomass burning effect on climate—heating or cooling?, *J. Climate*, 4, 578–588, 1991.
- Koren, I., Kaufman, Y. J., Remer, L. A., and Martins, J. V.: Measurement of the effect of Amazon smoke on inhibition of cloud formation, *Science*, 303, 1342–1345, doi:10.1126/science.1089424, 2004.
- 535 Koren, I., Kaufman, Y. J., Rosenfeld, D., Remer, L. A., and Rudich, Y.: Aerosol invigoration and restructuring of Atlantic clouds, *Geophys. Res. Lett.*, 32, L14 828, doi:10.1029/2005GL023187, 2005.
- Lamarque, J.-F., Bond, T. C., Eyring, V., Granier, C., Heil, A., Klimont, Z., Lee, D., Liousse, C., Mieville, A., Owen, B., Schultz, M. G., Shindell, D., Smith, S. J., Stehfest, E., Van Aardenne, J., Cooper, O. R., Kainuma, M., Mahowald, N., McConnell, J. R., Naik, V., Riahi, K., and van Vuuren, D. P.: Historical (18502000)
- 540 gridded anthropogenic and biomass burning emissions of reactive gases and aerosols: methodology and application, *Atmospheric Chemistry and Physics*, 10, 7017–7039, doi:10.5194/acp-10-7017-2010, 2010.
- Lamarque, J.-F., Emmons, L., Hess, P., Kinnison, D. E., Tilmes, S., Vitt, F., Heald, C., Holland, E. A., Lauritzen, P., Neu, J., Orlando, J., Rasch, P., and Tyndall, G. K.: CAM-chem: description and evaluation of interactive atmospheric chemistry in the Community Earth System Model, *Geosci. Model Devel.*, 5, 369–411, doi:
- 545 10.5194/gmd-5-369-2012, 2012.
- Langenfelds, R. L., Francey, R. J., Pak, B. C., Steele, L. P., Lloyd, J., Trudinger, C. M., and Allison, C. E.: Interannual growth rate variations of atmospheric CO₂ and its $\delta^{13}\text{C}$, H₂, CH₄, and CO between 1992 and 1999 linked to biomass burning, *Global Biogeochem. Cycles*, 16, 1048, doi:10.1029/2001GB001466, 2002.
- Lee, S., Kim, H. K., Yan, B., Cobb, C. E., Hennigan, C., Nichols, S., Chamber, M., Edgerton, E. S., Jansen,
- 550 J. J., Hu, Y., Zheng, M., Weber, R. J., and Russell, A. G.: Diagnosis of aged prescribed burning plumes impacting an urban area, *Environ. Sci. Technol.*, 42, 1438–1444, doi:10.1021/es7023059, 2008.
- Liu, H. and Randerson, J. T.: Interannual variability of surface energy exchange depends on stand age in a boreal forest fire chronosequence, *J. Geophys. Res.*, 113, G01 006, doi:10.1029/2007JG000483, 2008.
- Liu, X., Easter, R. C., Ghan, S. J., Zaveri, R., Rasch, P., Shi, X., Lamarque, J.-F., Gettelman, A., Morrison,
- 555 H., Vitt, F., Conley, A., Park, S., Neale, R., Hannay, C., Ekman, A. M. L., Hess, P., Mahowald, N., Collins, W., Iacono, M. J., Bretherton, C. S., Flanner, M. G., and Mitchell, D.: Toward a minimal representation of aerosols in climate models: description and evaluation in the Community Atmosphere Model CAM5, *Geosci. Model Devel.*, 5, 709–739, doi:10.5194/gmd-4-709-2012, 2012.
- Lu, J., Vecchi, G. A., and Reichler, T.: Expansion of the Hadley cell under global warming, *Geophys. Res. Lett.*,
- 560 34, L06 805, doi:10.1029/2006GL028443, 2007.
- Lu, J., Chen, G., and Frierson, D. M. W.: Response of the zonal mean atmospheric circulation to El Niño versus global warming, *J. Climate*, 21, 5835–5851, doi:10.1175/2008JCLI2200.1, 2008.
- Lyons, E. A., Jin, Y., and Randerson, J. T.: Changes in surface albedo after fire in boreal forest ecosystem of interior Alaska assessed using MODIS satellite observations, *J. Geophys. Res.*, 113, G02 012, doi:10.1029/
- 565 2007JG000606, 2008.
- Mahowald, N., Ward, D. S., Kloster, S., Flanner, M. G., Heald, C. L., Heavens, N. G., Hess, P. G., Lamarque, J.-F., and Chuang, P. Y.: Aerosol impacts on climate and biogeochemistry, *Annu. Rev. Environ. Resour.*, 36, 45–74, doi:10.1146/annurev-environ-042009-094507, 2011.
- Marlon, J. R., Bartlein, P. J., Carcaillet, C., Gavin, D. G., Harrison, S. P., Higuera, P. E., Joos, F., Power, M. J.,

- 570 and Prentice, I. C.: Climate and human influences on global biomass burning over the past two millennia, *Nature Geo.*, 1, 697–702, doi:10.1038/ngeo313, 2008.
- Martin, M. V., Logan, J. A., Leung, F.-Y., Nelson, D. L., and Diner, D. J.: Smoke injection heights from fires in North America: analysis of 5 years of satellite observations, *Atmos. Chem. Phys.*, 10, 1491–1510, doi:10.5194/acp-10-1491-2010, 2010.
- 575 Mitas, C. M. and Clement, A.: Has the Hadley cell been strengthening in recent decades?, *Geophys. Res. Lett.*, 32, L03 809, doi:10.1029/2004GL021765, 2005.
- Morton, D. C., DeFries, R. S., Nagol, J., Jr., C. M. S., Kasischke, E. S., Hurtt, G. C., and Dubayah, R.: Mapping canopy damage from understory fires in Amazon forests using annual time series of Landsat and MODIS data, *Remote Sensing of Environment*, 115, 1706 – 1720, doi:10.1016/j.rse.2011.03.002, 2011.
- 580 Myhre, G., Govaerts, Y., Haywood, J. M., Berntsen, T. K., and Lattanzio, A.: Radiative effect of surface albedo change from biomass burning, *Geophys. Res. Lett.*, 32, L20 812, doi:10.1029/2005GL022897, 2005.
- Neale, R. B., Chen, C.-C., Gettelman, A., Lauritzen, P. H., Park, S., Williamson, D. L., Conley, A. J., Garcia, R., Kinnison, D., Lamarque, J.-F., Marsh, D., Mills, M., Smith, A. K., Tilmes, S., Vitt, F., Morrison, H., Cameron-Smith, P., Collins, W. D., Iacono, M. J., Easter, R. C., Liu, X., and Taylor, M. A.: Description
585 of the NCAR Community Atmosphere Model (CAM 5.0), Tech. rep., National Center for Atmospheric Research, 2010.
- Neelin, J. D., Munnich, M., Su, H., Meyerson, J. E., and Holloway, C. E.: Tropical drying trends in global warming models and observations, *Proc. Nat. Acad. Sci.*, 103, 6110–6115, doi:10.1073/pnas.0601798103, 2006.
- 590 Ohara, T., Akimoto, H., Kurokawa, J., Horii, N., Yamaji, K., Yan, X., and Hayasaka, T.: An Asian emission inventory of anthropogenic emission sources for the period 1980–2020, *Atmospheric Chemistry and Physics*, 7, 4419–4444, doi:10.5194/acp-7-4419-2007, 2007.
- Oort, A. H. and Yienger, J. J.: Observed interannual variability in the Hadley Circulation and its connection to ENSO, *J. Climate*, 9, 2751–2767, 1996.
- 595 Page, S. E., Siegert, F., Rieley, J. O., Boehm, H. D., Jaya, A., and Limin, S.: The amount of carbon released from peat and forest fires in Indonesia during 1997, *Nature*, 420, 61–65, doi:10.1038/nature01131, 2002.
- Penner, J. E., Dickison, R. E., and O'Neill, C. A.: Effects of aerosol from biomass burning on the global radiation budget, *Science*, 256, 1432–1434, doi:10.1126/science.256.5062.1432, 1992.
- Power, M. J., Marlon, J., Ortiz, N., Bartlein, P. J., Harrison, S. P., Mayle, F. E., Ballouche, A., Bradshaw,
600 R. H. W., Carcaillet, C., and Cordova, C.: Changes in fire regimes since the Last Glacial Maximum: an assessment based on a global synthesis and analysis of charcoal data, *Clim. Dyn.*, 30, 887–907, doi:10.1007/s00382-007-0334-x, 2008.
- Quan, X.-W., Diaz, H. F., and Hoerling, M. P.: Change of the tropical Hadley cell since 1950, *Kluwer Academic Publishers*, 2005.
- 605 Ramanathan, V. and Carmichael, G.: Global and regional climate changes due to black carbon, *Nature Geo.*, 1, 221–227, doi:10.1038/ngeo156, 2008.
- Ramanathan, V., Crutzen, P. J., Kiehl, J. T., and Rosenfeld, D.: Aerosols, climate, and the hydrological cycle, *Science*, 294, 2119–2124, 2001.
- Randerson, J. T., Chen, Y., van der Werf, G. R., Rogers, B. M., and Morton, D. C.: Global burned area and

- 610 biomass burning emissions from small fires, *J. Geophys. Res.*, 117, G04012, doi:10.1029/2012JG002128, 2012.
- Rasch, P. J., Collins, W. D., and Eaton, B. E.: Understanding the Indian Ocean Experiment (INDOEX) aerosol distributions with an aerosol assimilation, *J. Geophys. Res.*, 106, 7337–7355, 2001.
- Reid, J. S., Koppman, R., Eck, T. F., and Eleuterio, D. P.: A review of biomass burning emissions part II:
615 Intensive physical properties of biomass burning particles, *Atmos. Chem. Phys.*, 3, 799–825, 2005.
- Reid, J. S., Hyer, E. J., Prins, E. M., Westphal, D. L., Zhang, J., Wang, J., Christopher, S. A., Curtis, C. A., Schmidt, C. C., Eleuterio, D. P., Richardson, K. A., and Hoffman, J. P.: Global monitoring and forecasting of biomass-burning smoke: Description of and lessons from the Fire Locating and Modeling of Burning Emissions (FLAMBE) program, *IEEE J. Appl. Earth. Obs. Rem. Sens.*, 2, 144–162, 2009.
- 620 Rosenfeld, D.: TRMM observed first direct evidence of smoke from forest fires inhibiting rainfall, *Geophys. Res. Lett.*, 26, 3105, 1999.
- Rosenfeld, D.: Aerosols, clouds, and climate, *Science*, 312, 1323–1324, doi:10.1126/science.1128972, 2006.
- Rosenfeld, D., Woodley, W. L., Axisa, D., Freud, E., Hudson, J. G., and Givati, A.: Aircraft measurements of the impacts of pollution aerosols on clouds and precipitation over the Sierra Nevada, *J. Geophys. Res.*, 113,
625 D15 203, doi:10.1029/2007JD009544, 2008.
- Sitch, S., Cox, P. M., Collins, W. J., and Huntingford, C.: Indirect radiative forcing of climate change through ozone effects on the land-carbon sink, *Nature*, 448, 791–794, doi:10.1038/nature06059, 2007.
- Spessa, A., McBeth, B., and Prentice, C.: Relationships among fire frequency, rainfall and vegetation patterns in the wet-dry tropics of northern Australia: an analysis based on NOAA-AVHRR data, *Global Ecology and*
630 *Biogeography*, 14, 439–454, doi:10.1111/j.1466-822x.2005.00174.x, 2005.
- Swetnam, T. W. and Betancourt, J. L.: Mesoscale disturbance and ecological response to decadal climatic variability in the American Southwest, *J. Climate*, 11, 3128–3147, 1998.
- Tosca, M. G., Randerson, J. T., Zender, C. S., Flanner, M. F., and Rasch, P. J.: Do biomass burning aerosols intensify drought in Equatorial Asia during El Niño?, *Atmos. Phys. Chem.*, 10, 3515–3528, doi:10.5194/
635 *acp-10-3515-2010*, 2010., 2010.
- Tosca, M. G., Randerson, J. T., Zender, C. S., Nelson, D. L., Diner, D. J., and Logan, J. A.: Dynamics of fire plumes and smoke clouds associated with peat and deforestation fires in Indonesia, *J. Geophys. Res.*, 116,
D08 207, doi:10.1029/2010JD015148, 2011.
- Turetsky, M. R., Kane, E. S., Harden, J. W., Ottmar, R. D., and Manies, K. L.: Recent acceleration of biomass
640 burning and carbon losses in Alaskan forests and peatlands, *Nature Geosci.*, 4, 27–31, 2011.
- van der Werf, G. R., Randerson, J. T., Giglio, L., Collat, G. T., Kasibhatla, P. S., and Arellano Jr., A. S.: Interannual variability in global biomass burning emissions from 1997 to 2004, *Atmos. Chem. and Phys.*, 6,
3423–3441, 2006.
- van der Werf, G. R., Dempewolf, J., Trigg, S. N., Randerson, J. T., Giglio, L., Murdiyarso, D., Peters, W.,
645 Morton, D. C., Collatz, G. J., Dolman, A. J., and DeFries, R. S.: Climate regulation of fire emissions and deforestation in equatorial Asia, *Proc. Natl. Acad. Sci.*, 105, 20 350–20 355, doi:10.1073/pnas.0803375105, 2008.
- van der Werf, G. R., Randerson, J. T., Giglio, L., Collatz, G. J., Mu, M., Kasibhatla, P. S., Morton, D. C., DeFries, R. S., Jin, Y., and van Leeuwen, T. T.: Global fire emissions and the contribution of deforestation,

- 650 savanna, forest, agricultural, and peat fires (1997-2009), *Atmos. Chem. and Phys.*, 10, 11 707–11 735, doi: 10.5194/acp-10-11707-2010, 2010.
- Wang, H., Easter, R. C., Rasch, P. J., Wang, M., Liu, X., Ghan, S. J., Qian, Y., Yoon, J.-H., Ma, P.-L., and Velu, V.: Sensitivity of remote aerosol distributions to representation of cloud-aerosol interactions in a global climate model, *Geosci. Mod. Dev. Discuss.*, 6, 331–378, doi:10.5194/gmdd-6-331-2013, 2013.
- 655 Ward, D. S., Kloster, S., Mahowald, N. M., Rogers, B. M., Randerson, J. T., and Hess, P. G.: The changing radiative forcing of fires: global model estimates for past, present and future, *Atmos. Chem. Phys.*, 12, 10 857–10 886, doi:10.5194/acpd-12-10857-2012, 2012.
- Westerling, A. L., Hidalgo, H. G., Cayan, D. R., and Swetnam, T. W.: Warming and earlier spring increase western U.S. forest wildfire activity, *Science*, 313, 940–943, doi:10.1126/science.1128834, 2006.
- 660 Xian, P., Reid, J., Turk, J., Hyer, E., and Westphal, D.: Impact of modeled versus satellite measured tropical precipitation on regional smoke optical thickness in an aerosol transport model, *Geophys. Res. Lett.*, 36, L16 805, doi:10.1029/2009GL038823, 2009.
- Yoshimori, M. and Broccoli, A. J.: On the link between Hadley circulation changes and radiative feedback processes, *Geophys. Res. Lett.*, 36, L20 703, doi:10.1029/2009GL040488, 2009.
- 665 Zhang, Y., Fu, R., Yu, H., Qian, Y., Dickinson, R., Dias, M. A. F. S., da Silva Dias, P. L., and Fernandes, K.: Impact of biomass burning aerosol on the monsoon circulation transition over Amazonia, *Geophys. Res. Lett.*, 36, L10 814, doi:10.1029/2009GL037180, 2009.

Table 1. Summary of scaling factors for selected biomass burning regions

	Region			
	South America ¹	southern Africa ²	equatorial Asia ³	boreal North America ⁴
Original sum of BC and OC emissions ⁵ (Tg yr ⁻¹)	3.5	4.8	3.3	1.6
Number of months contributing to 80% of emissions (out of 156)	29	31	18	11
MODIS scalar	3.03	2.56	1.75	1.87
MODIS correlation (r ²)	0.71	0.78	0.67	0.88
MISR scalar	1.77	1.63	1.59	1.02
MISR correlation (r ²)	0.71	0.73	0.71	0.84
AVERAGE (MISR and MODIS) scalar	2.40	2.10	1.67	1.45
Adjusted sum of BC and OC emissions ^a (Tg yr ⁻¹)	8.5	10.0	5.6	2.3

¹ South America (SAM), region bounded by 25°S-0, 65°W-40°W.

² southern Africa (SAF), region bounded by 15°S-5°S, 10°E-30°E.

³ equatorial Asia (EAS), region bounded by 10°S-7°N, 90°E-150°E.

⁴ boreal North America (BNA), region bounded by 50°N-70°N, 170°W-90°W.

⁵ **The original BC and OC emissions were 2x GFEDv3** (van der Werf et al., 2010).

Table 2. Global BC and OC scalars and emissions from satellite-based optimization.

GFED Region ¹	Aerosol emissions scalar	Sum of OC and BC emissions from 2xGFEDv3 (Tg yr ⁻¹)	Adjusted sum of OC and BC emissions (Tg yr ⁻¹)
SHSA	2.40	5.3	12.8
NHSA	same as SHSA	0.4	1.0
CEAM	same as SHSA	0.4	1.1
SHAF	2.10	10.3	21.6
NHAF	same as SHAF	8.3	17.4
EURO	same as SHAF	0.09	0.21
AUST	same as SHAF	2.4	5.0
EQAS	1.67	3.6	6.1
SEAS	same as EQAS	2.1	3.5
CEAS	same as EQAS	0.7	1.3
MIDE	same as EQAS	0.03	0.05
BONA	1.45	2.1	3.0
BOAS	same as BONA	4.5	6.5
TENA	same as BONA	0.3	0.4
global total	1.97	40.6	79.9

¹ GFED regions defined as in van der Werf et al. (2006)

SHSA = southern hemisphere South America, NHSA = northern hemisphere South America, CEAM = central America, SHAF = southern hemisphere Africa, NHAF = northern hemisphere Africa, EURO = Europe, AUST = Australia, EQAS = equatorial Asia, SEAS = southeast Asia CEAS = central Asia, MIDE = Middle East, BONA = boreal North America, BOAS = boreal Asia, TENA = temperate North America

Table 3. Comparison of optical depths from simulations with original and adjusted GFEDv3 emissions

Region		Observed	Modeled		Percent (%)
			(original emissions)	(adjusted emissions)	change
South America (SA)	MISR	0.141	0.121	0.152	26
	MODIS	0.140	0.124	0.158	27
	AERONET*	0.301	0.112	0.259	129
southern Africa (SAF)	MISR	0.258	0.189	0.289	53
	MODIS	0.278	0.186	0.287	54
	AERONET	0.253	0.124	0.207	71
equatorial Asia (EAS)	MISR	0.160	0.089	0.090	1
	MODIS	0.155	0.093	0.095	2
	AERONET	0.190	0.109	0.151	47
boreal North America (BNA)	MISR	0.124	0.051	0.055	8
	MODIS	0.136	0.058	0.062	7
	AERONET	–	–	–	–

* AERONET optical depths are only those where greater than 30% of the AOD simulated by CAM5 is from fire.

Regions are the same as those in Table 4.1

Table 4. Summary of the simulated global climate response to fire aerosols

Earth System variable	NOFIRE (control)	FIRE–NOFIRE (C.I. ^a)	% change
Global			
Aerosol optical depth	0.15	+0.02 (0.002)	+10
Top-of-atmosphere radiative forcing (W m^{-2})	-0.47	+0.18 (0.10)	
Net surface shortwave radiation (W m^{-2})	155.3	-1.3 (0.2)	-1
Surface air temperature ($^{\circ}\text{C}$)	14.8	-0.13 (0.01)	
Precipitation (mm d^{-1})	2.88	-0.03 (0.003)	-1
Mean maximum annual NH ψ ($\times 10^{10} \text{ kg s}^{-1}$) ^b	8.8	-0.1 (0.1)	-1
Mean maximum DJF NH ψ ($\times 10^{10} \text{ kg s}^{-1}$)	23	-0.3 (0.2)	-1
Width of NH Hadley Cell ($\Delta\phi^{\circ}$)	31.3	+0.4 (0.4)	+1
South America (SA) ^c			
Aerosol optical depth	0.09	+0.08 (0.02)	+91
Net surface shortwave radiation (W m^{-2})	215.7	-9.1 (1.8)	-4
Surface air temperature ($^{\circ}\text{C}$)	26.7	-0.37 (0.07)	
Precipitation (mm d^{-1})	3.62	-0.08 (0.05)	-2
southern Africa (SAF)			
Aerosol optical depth	0.10	+0.19 (0.03)	+199
Net surface shortwave radiation (W m^{-2})	243.2	-19.1 (3.2)	-8
Surface air temperature ($^{\circ}\text{C}$)	24.0	-0.46 (0.07)	
Precipitation (mm d^{-1})	3.32	-0.24 (0.05)	-7

^aC.I. = 95% confidence interval (standard error $\times 1.96$)

^bDefined as the change in the maximum northern hemisphere ψ (horizontally and vertically varying) between the two simulations

^c South America and southern Africa regions as defined in Table 1.

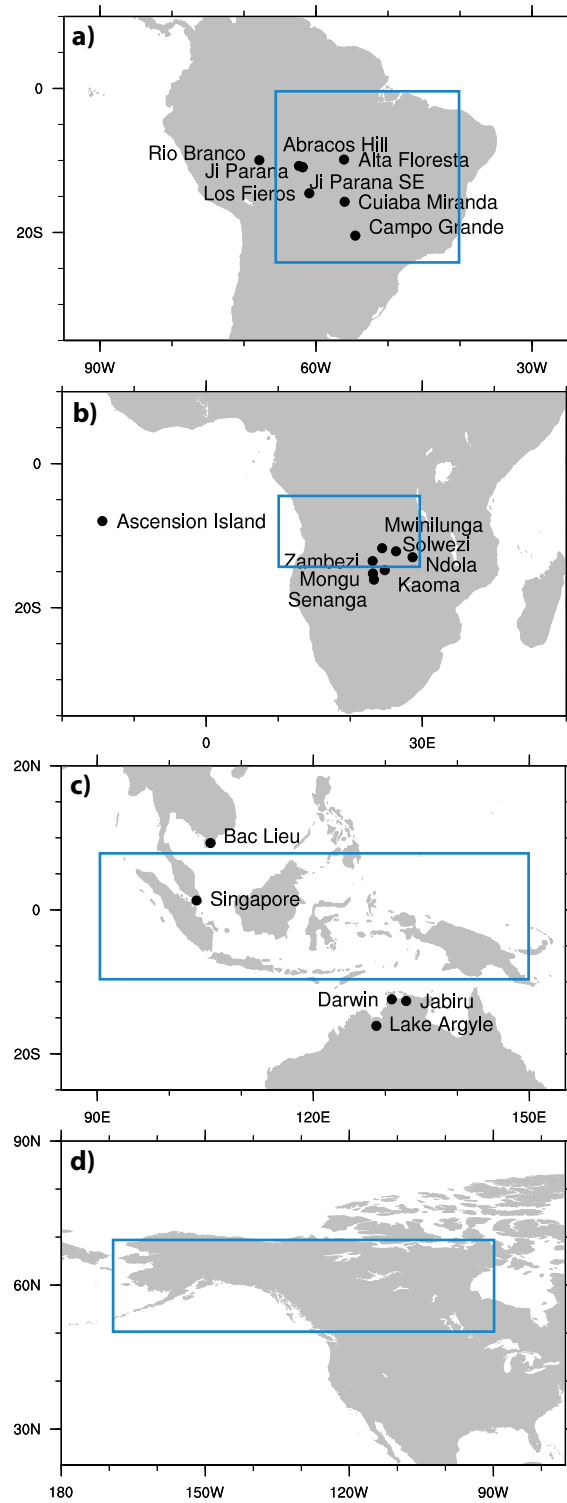


Fig. 1. Regional maps of AERONET stations (black dots) and MISR/MODIS scaling areas (blue boxes) for a) South America (SA), b) southern Africa (SAF), c) equatorial Asia (EAS) and d) boreal North America (BNA). There were no suitable AERONET stations in BNA.

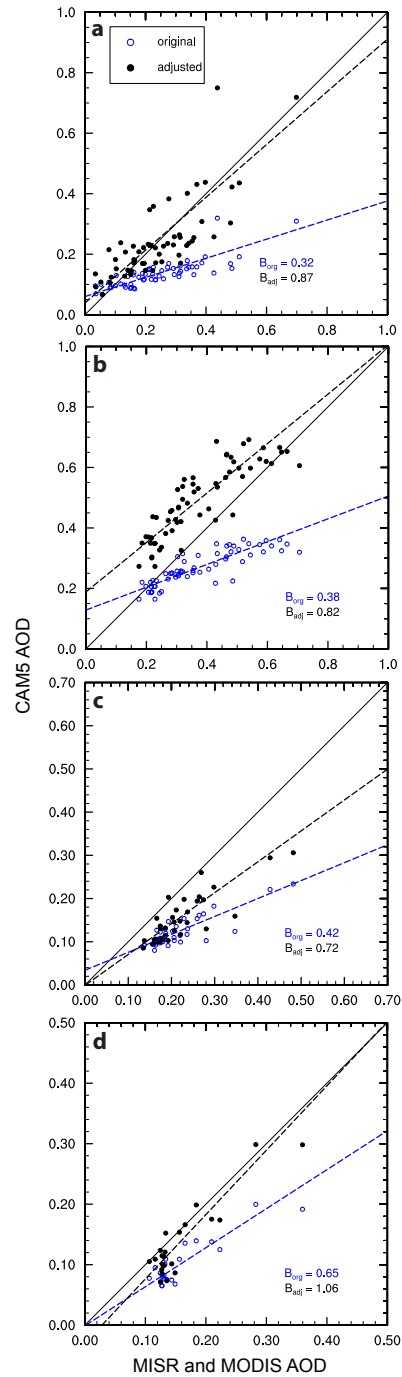


Fig. 2. Linear relations between CAM5-simulated aerosol optical depths (y-axis) and MISR-MODIS optical depths (x-axis) for unadjusted case (blue dots/line) and adjusted case (black dots/line) emissions cases. Regression slopes for the original emissions (B_{orig}) and adjusted emissions (B_{adj}) model simulations are shown in each panel. The three regions shown are: a) South America (SA; 25°S:0, 40:65°W), b) southern Africa (SAF; 15:5°S,10:30°E) c) Equatorial Asia (EAS; 10°S:7°N, 90:150°E), and d) boreal North America (BNA; 50°N:70°N, 170:90°W). Only those months that cumulatively contributed 80% of regional emissions from 1997-2009 were included in the analysis. Correlation coefficients (r^2) were 0.65 (unadj.) and 0.62 (adj.) for SA, 0.72 (unadj.), 0.55 (adj.) for SAF, 0.69 (unadj.) and 0.71 (adj.) for EAS, and 0.78 (unadj.) and 0.83 (adj.) for BNA.

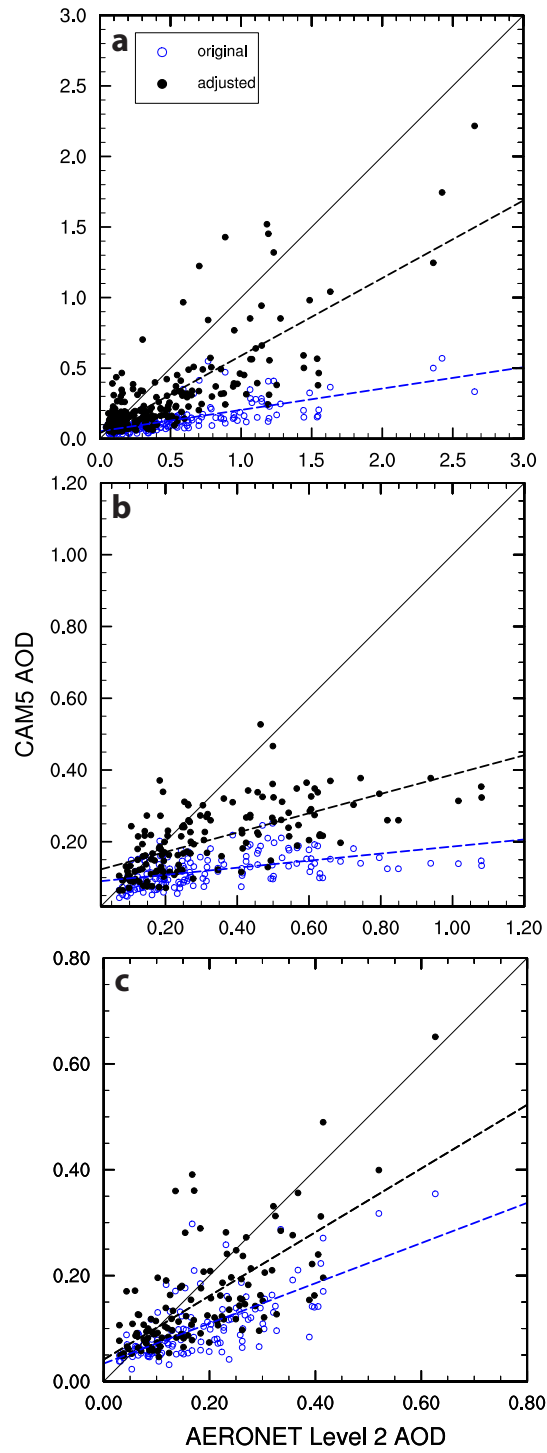


Fig. 3. Linear relations between CAM5-simulated aerosol optical depths (y-axis) and AERONET optical depths (x-axis) for the unadjusted case (blue dots/line) and adjusted case (black dots/line), showing better agreement in the adjusted scenario. Regions are the same as Fig. 2: a) South America (SA), b) southern Africa (SAF) and c) equatorial Asia (EA). Only those months where CAM5 AOD from fire emissions was greater than or equal to 30% were used in our comparisons.

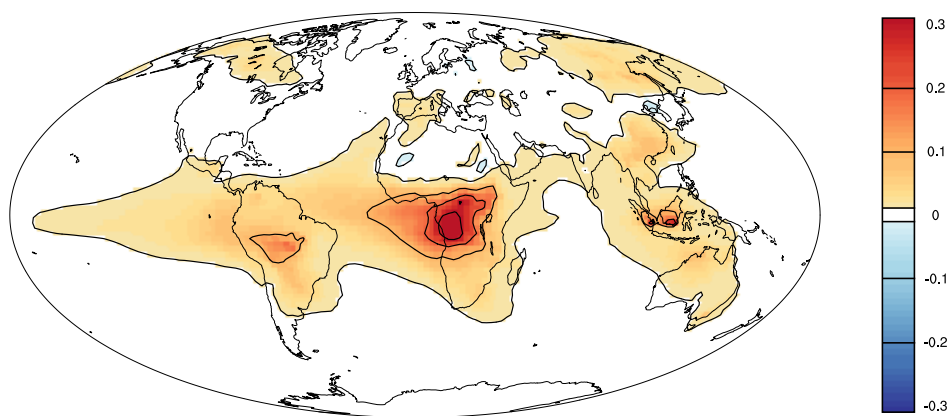


Fig. 4. Global map of aerosol optical depth anomalies (FIRE minus NOFIRE) from the CAM5 simulations. Averages were calculated using all 52 years from each simulation (and excluding the preceding spinup periods). This applies to all remaining figures and tables.

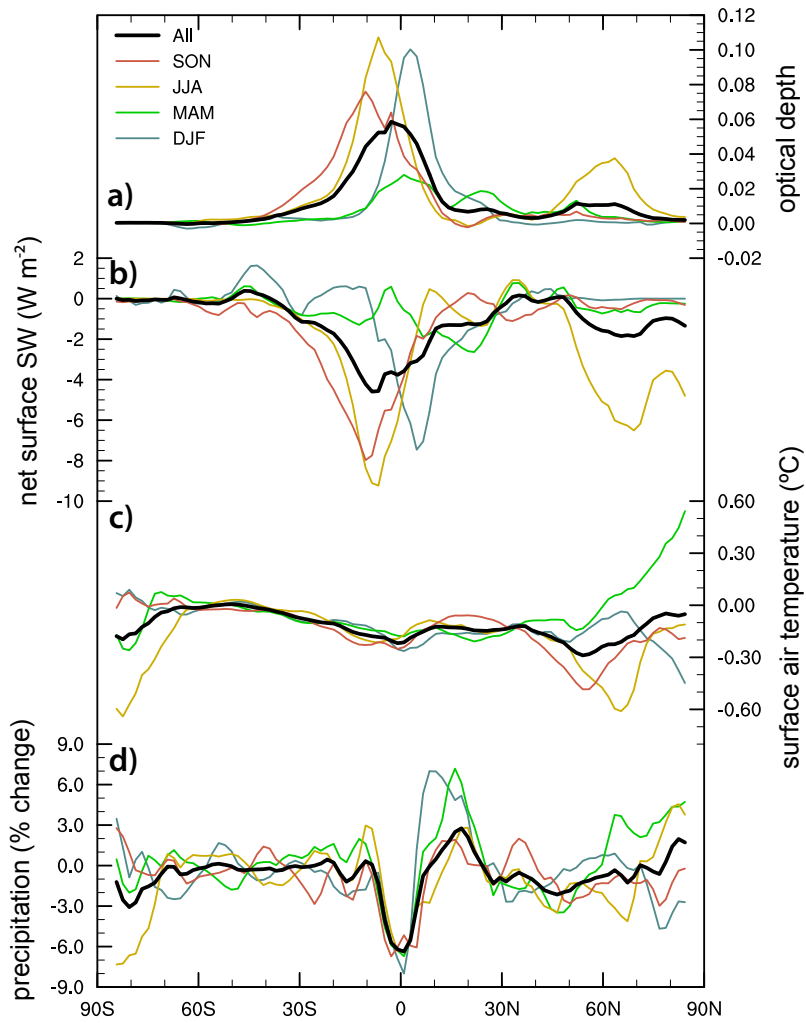


Fig. 5. Zonally averaged climate anomalies (FIRE - NOFIRE) from CAM5 simulations: a) aerosol optical depth, b) net insolation (W m^{-2}), c) temperature ($^{\circ}\text{C}$), and d) precipitation (percent (%) change). Thin lines are seasonal averages, thick lines are annual averages.

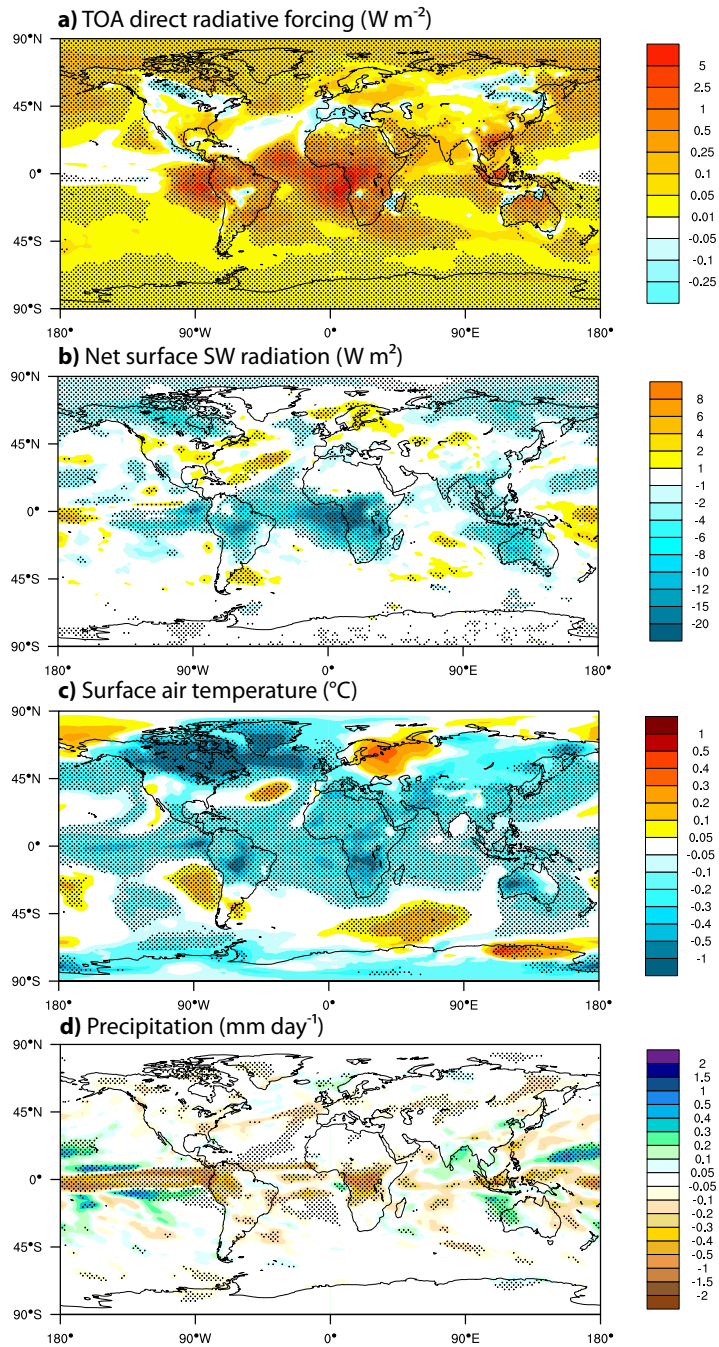


Fig. 6. Global maps of climate anomalies (FIRE minus NOFIRE for (b) - (d) only) from CAM5 simulations: a) top of atmosphere radiative forcing ($W m^{-2}$ (from FIRE run only), b) net insolation ($W m^{-2}$), (c) surface air temperature ($^{\circ}C$), and d) precipitation ($mm d^{-1}$). Dotted stippling of statistical significance (95%). Significance was determined by computing the t-test statistic at each grid cell for $\alpha=0.05$. Surface air temperature was the mean mid-layer air temperature in the lowest atmospheric level of the model.

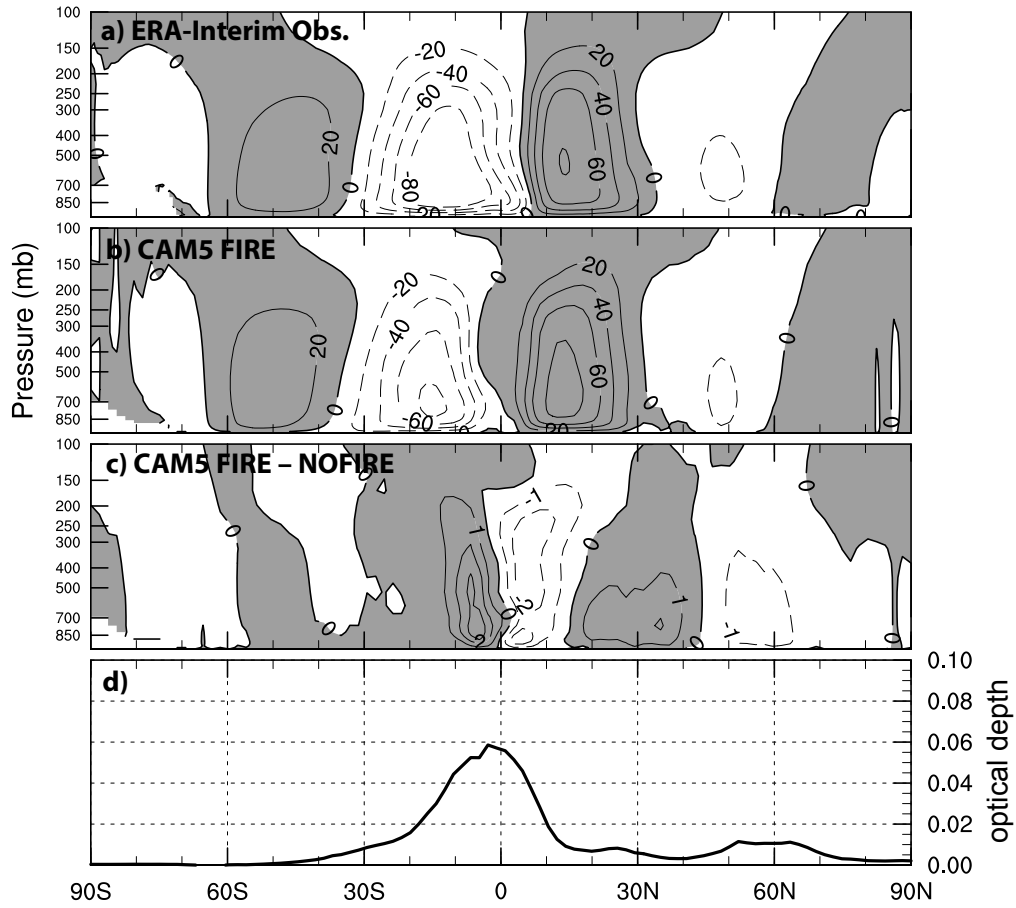


Fig. 7. Zonal-mean (annual) mass streamfunction (ψ) derived from a) ECMWF ERA-interim observations, b) CAM5 simulations including fire aerosols, and c) the difference between the FIRE and NOFIRE simulations. Units are in 10^9 kg s^{-1} for all plots. Contour intervals vary. Shaded regions indicate northward transport, un-shaded regions are southward transport. d) is the zonally averaged AOD.

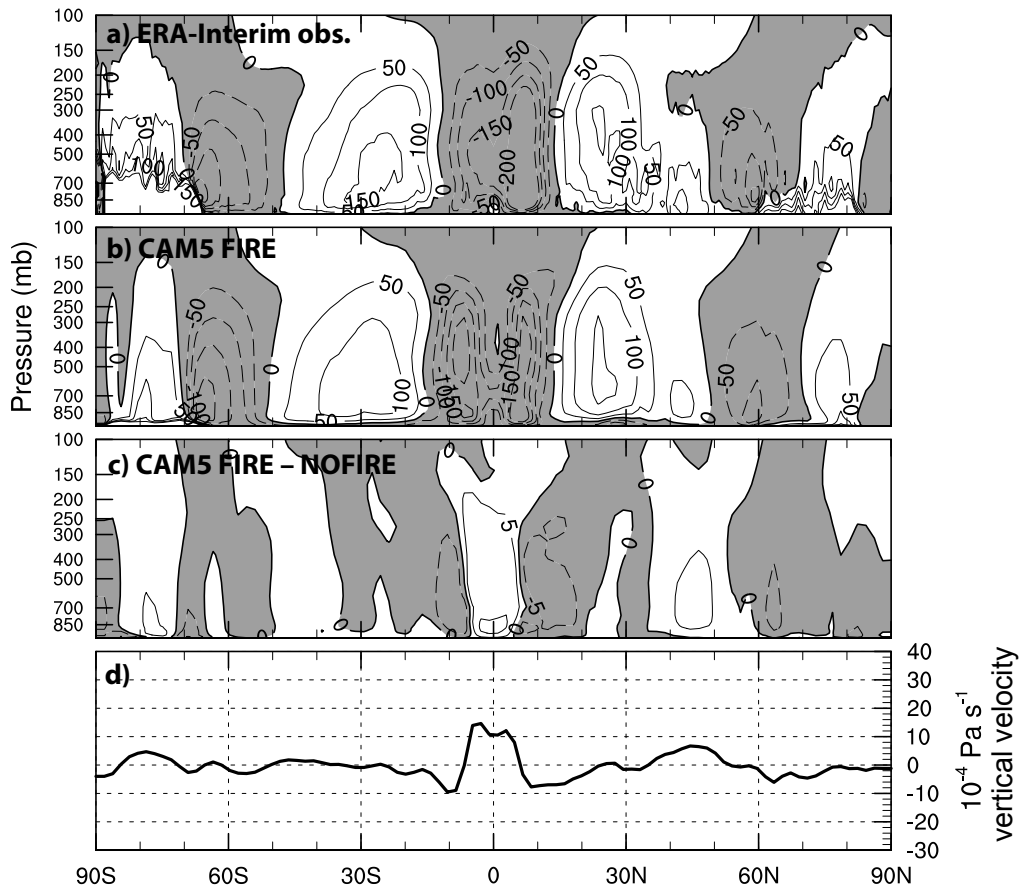


Fig. 8. Zonal-mean (annual) vertical velocities (ω) derived from a) ECMWF ERA-interim observations, b) CAM5 simulations including fire aerosols, and c) the difference between the FIRE and NOFIRE simulations. Units are in $10^{-4} \text{ Pa s}^{-1}$ for all plots. Contour intervals vary. Negative values (shaded regions) indicate upward velocities, positive values (un-shaded regions) are downward velocities. d) is the 500mb vertical velocity anomalies (as in (c)).

Figure S1. Global maps of aerosol optical depth (AOD). (a) MISR-observed AOD for 2001—2009, (b) the difference between CAM5-simulated AOD and MISR for the unadjusted emissions scenario and (c) the difference between CAM5 AOD and MISR for the adjusted emissions scenario. Note the improvement in fire regions of Africa, South America and equatorial Asia.

Figure S2. Time series of modeled (CAM5) AODs for simulations with adjusted fire emissions for the three main burning regions of (a) South America, (b) southern Africa, (c) equatorial Asia and (d) boreal North America (for lat-lon boxes, see Fig. 1 in the main text). The thick line represents the total AOD and the thin line is the fire-only AOD (the difference in AOD between the FIRE and NOFIRE simulations).

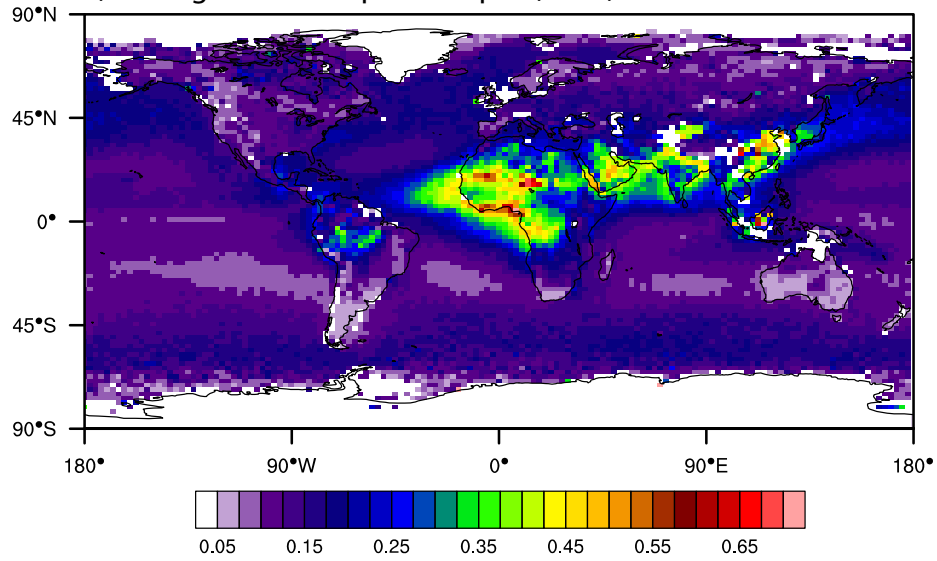
Figure S3. Time series of modeled (CAM5) and observed (MISR & MODIS, combined) AODs for the same regions as Figure S2. The dashed lines are observations, the thin lines are from simulations with unadjusted emissions and the thick lines from simulations with adjusted fire emissions.

Figure S4. (a) Global map of anomalies (FIRE – NOFIRE) of the difference in temperature between the surface and 700 mb. (b) Global map of vertical velocity anomalies (FIRE – NOFIRE) at 850 mb (10^{-3} Pa s⁻¹)

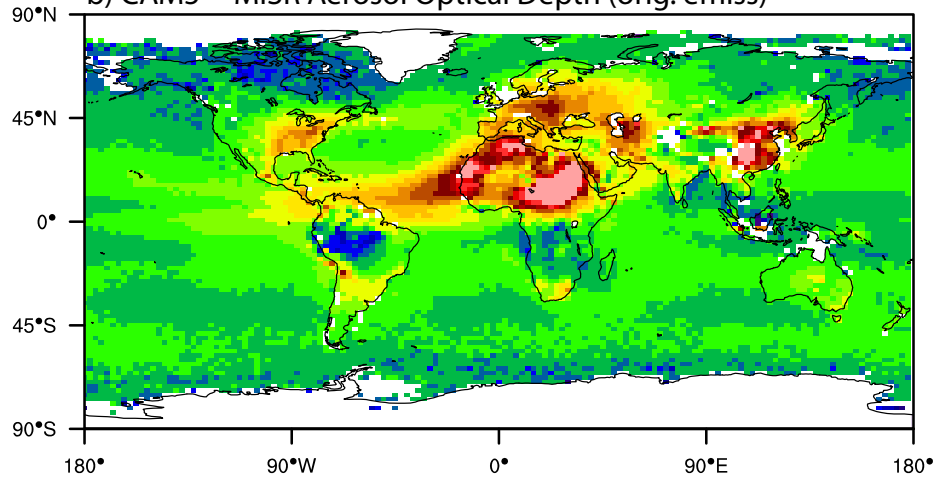
Figure S5. A cross-section of May–October vertical profiles of zonally averaged anomalies (FIRE – NOFIRE) over central Africa (40°S–40°N) for (a) atmospheric heating rates (10^6 K s⁻¹), (b) temperature (°C), and (c) vertical velocities (10^{-5} Pa s⁻¹). Zonally averaged AOD anomalies are shown in (d) for the same region and period.

Figure S6. A cross-section of annually averaged vertical profiles of zonally averaged anomalies (FIRE – NOFIRE) over the central Pacific for (a) atmospheric heating rates ($\times 10^{-7}$ K s⁻¹), and (b) vertical velocities (10^{-5} Pa s⁻¹). Zonally averaged sea surface temperature (SST) anomalies are shown in (d) for the same region and period.

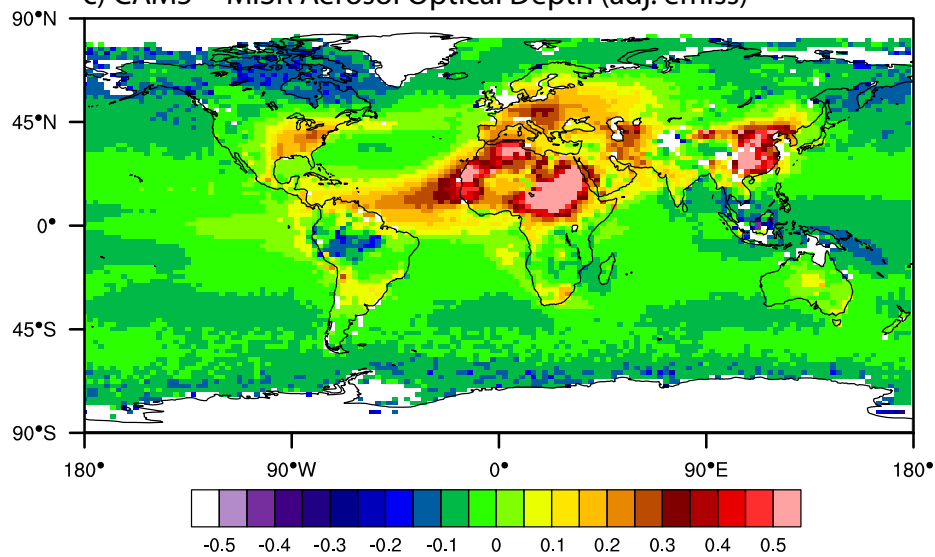
a) Average Aerosol Optical Depth (MISR)



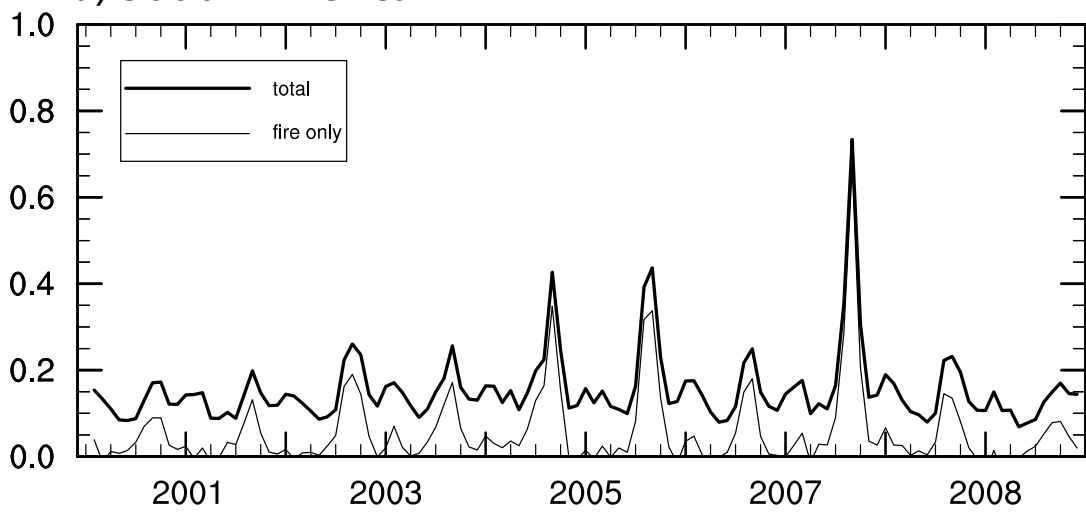
b) CAM5 -- MISR Aerosol Optical Depth (orig. emiss)



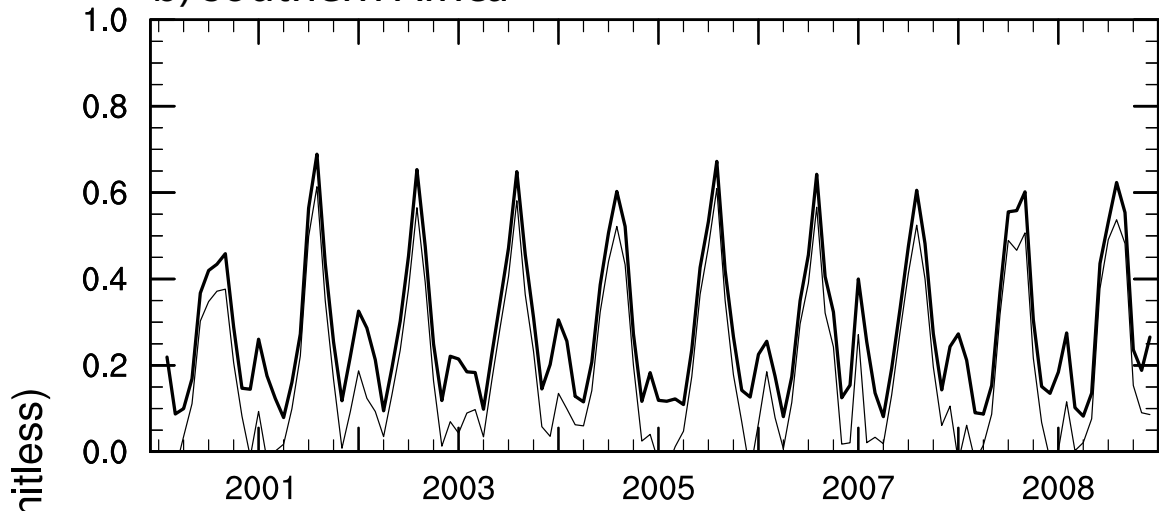
c) CAM5 -- MISR Aerosol Optical Depth (adj. emiss)



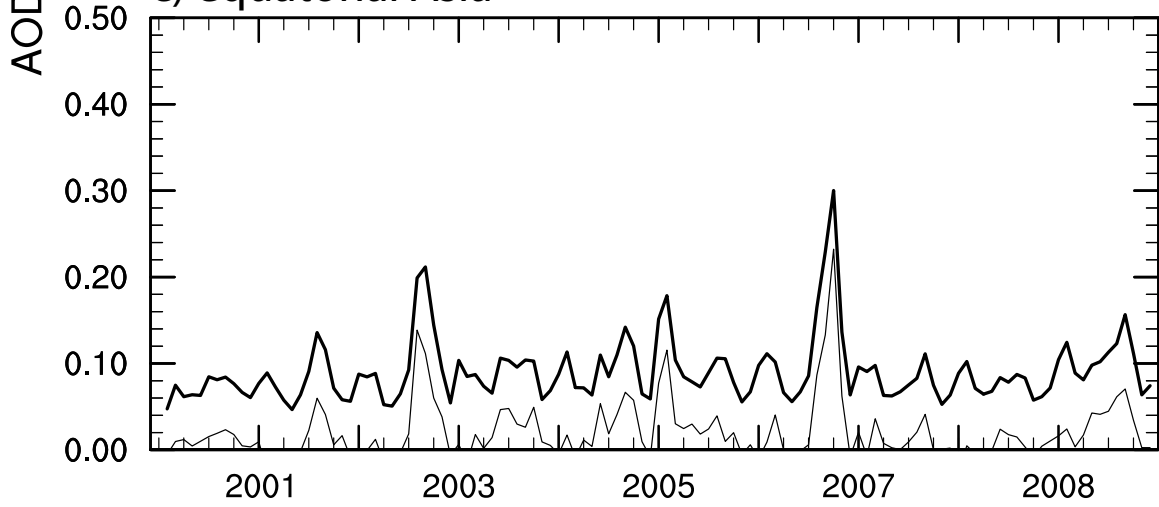
a) South America



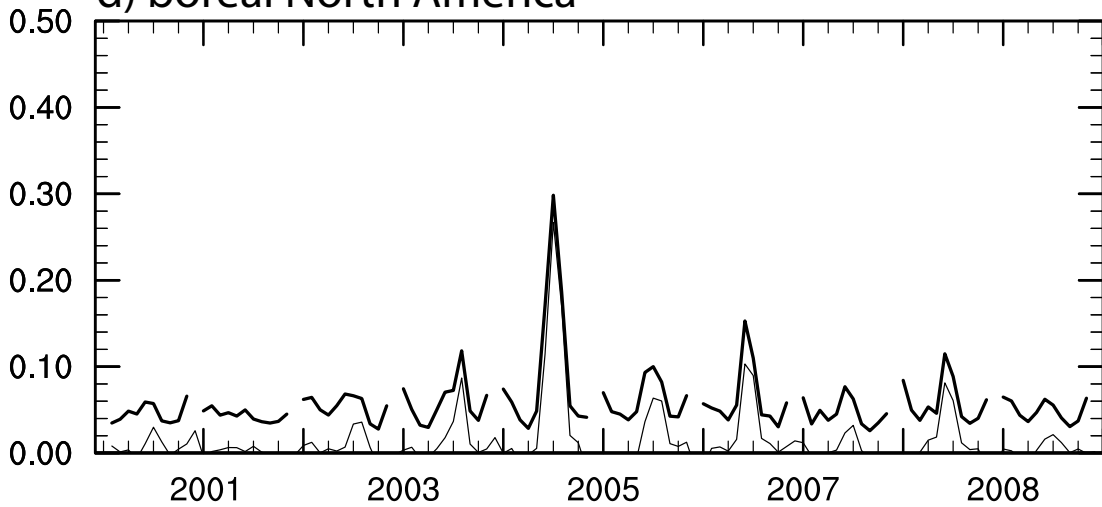
b) southern Africa



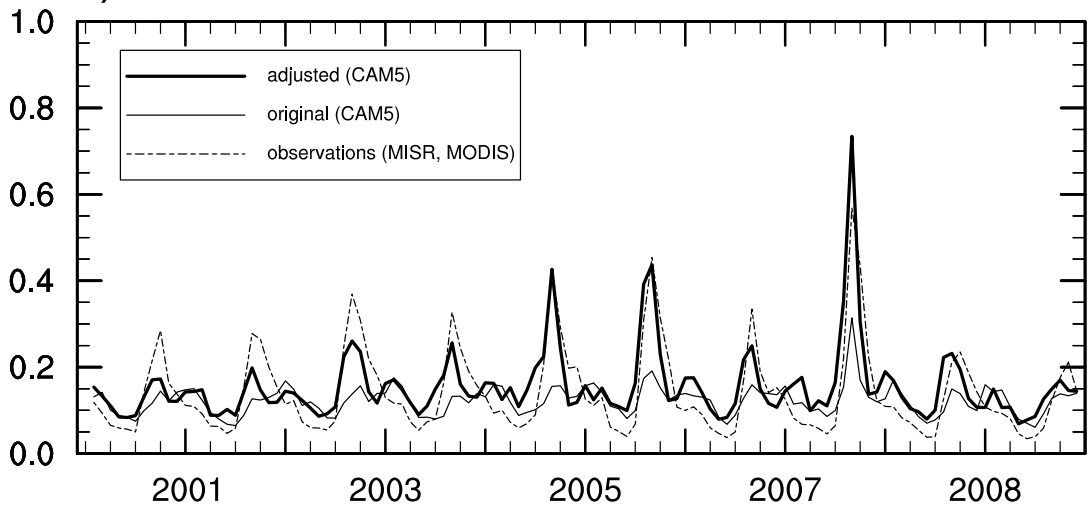
c) equatorial Asia



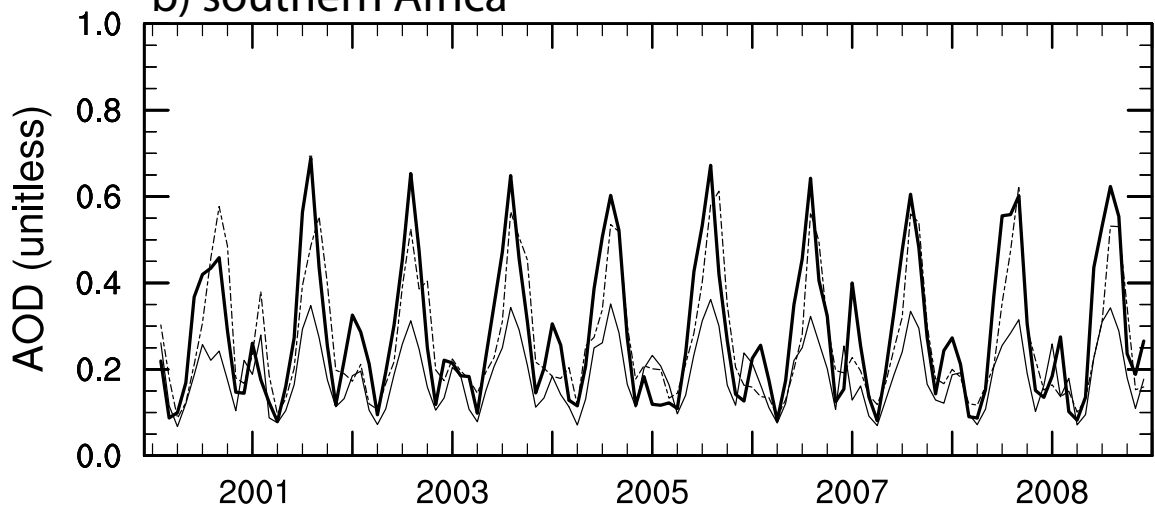
d) boreal North America



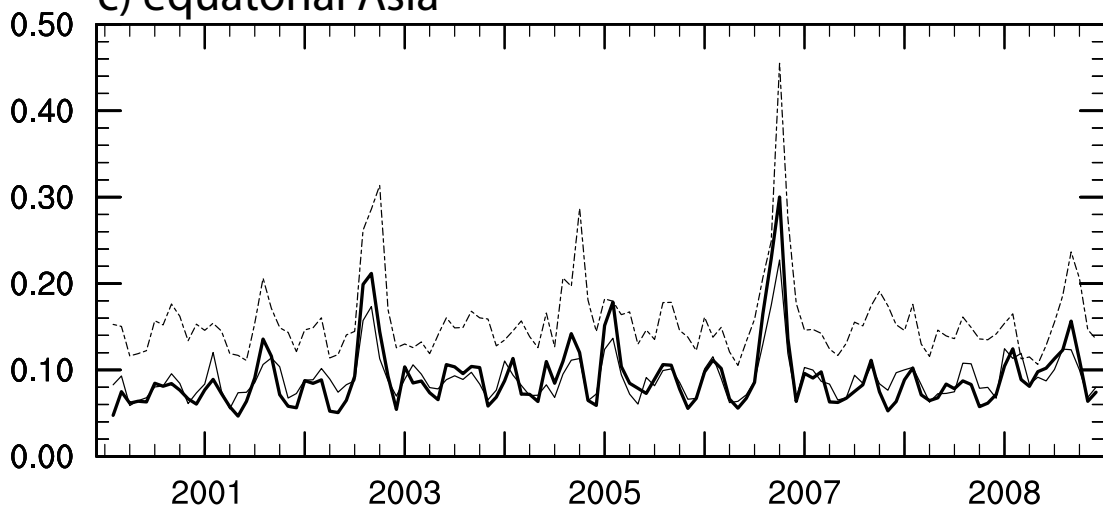
a) South America



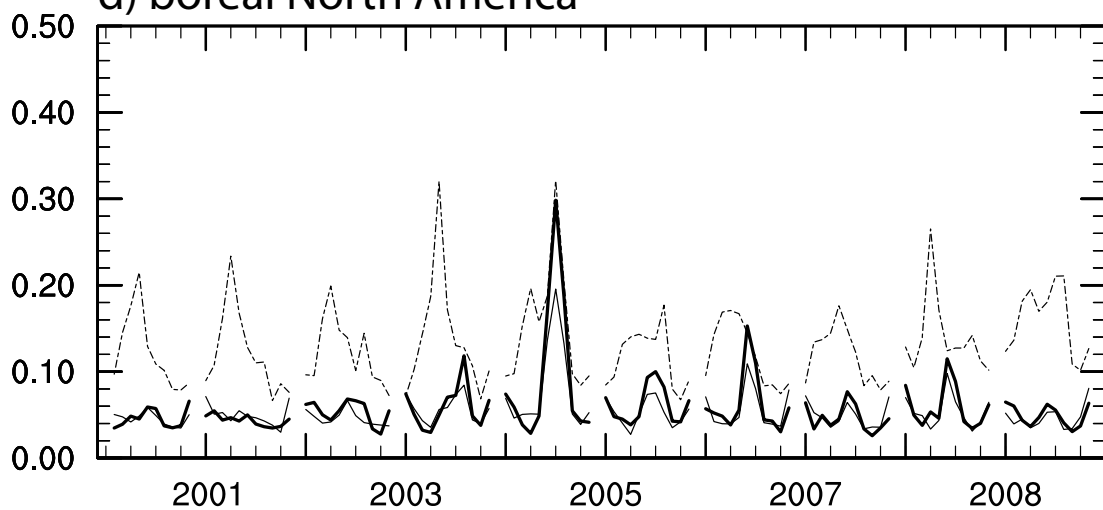
b) southern Africa



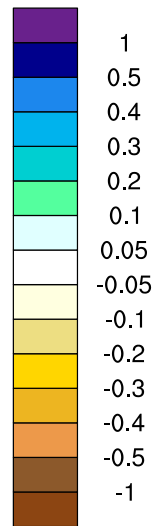
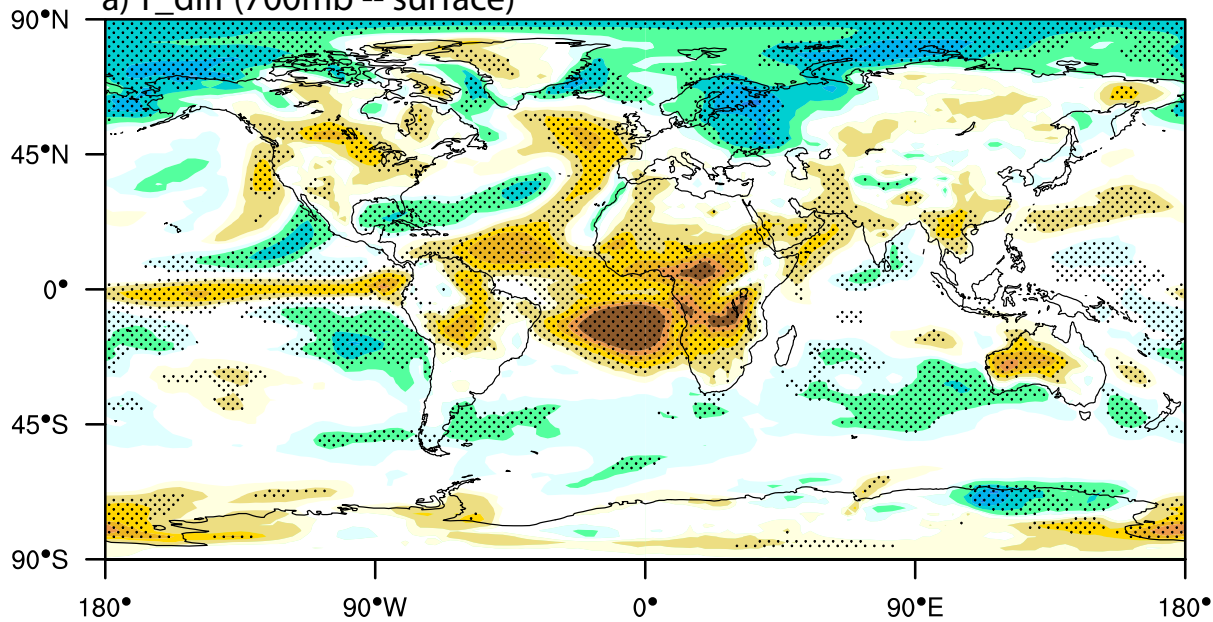
c) equatorial Asia



d) boreal North America



a) T_diff (700mb -- surface)



b) 500 mb vertical velocity (omega)

